



HAL
open science

Multimodal PET/PAI/FLI imaging probe based on meso-O-alkyl heptamethine cyanine: Synthesis, [18F]F-radiolabelling and photophysical characterizations

Kamal Jouad, Emilien Mengel, Katalin Selmeczi, Mathilde Bouché, Charlotte Collet-Defossez, Nadia Pellegrini Moïse, Sandrine Lamandé-Langle

► To cite this version:

Kamal Jouad, Emilien Mengel, Katalin Selmeczi, Mathilde Bouché, Charlotte Collet-Defossez, et al.. Multimodal PET/PAI/FLI imaging probe based on meso-O-alkyl heptamethine cyanine: Synthesis, [18F]F-radiolabelling and photophysical characterizations. *Dyes and Pigments*, 2024, 223, pp.111995. 10.1016/j.dyepig.2024.111995 . hal-04454881

HAL Id: hal-04454881

<https://hal.univ-lorraine.fr/hal-04454881v1>

Submitted on 13 Nov 2024

HAL is a multi-disciplinary open access archive for the deposit and dissemination of scientific research documents, whether they are published or not. The documents may come from teaching and research institutions in France or abroad, or from public or private research centers.

L'archive ouverte pluridisciplinaire **HAL**, est destinée au dépôt et à la diffusion de documents scientifiques de niveau recherche, publiés ou non, émanant des établissements d'enseignement et de recherche français ou étrangers, des laboratoires publics ou privés.

Multimodal PET/PAI/FLI imaging probe based on meso-*O*-alkyl heptamethine cyanine: Synthesis, ¹⁸F-radiolabelling and photophysical characterizations

Kamal Jouad^{a,1}, Emilien Mengel^{a,1}, Katalin Selmeczi^a, Mathilde Bouché^a, Charlotte Collet-Defossez^{b,c}, Nadia Pellegrini Moïse^{a,*}, Sandrine Lamandé-Langle^{a,*}

^a *Université de Lorraine, CNRS, L2CM, F-54000 Nancy, France*

^b *NancycloTEP, Molecular Imaging Platform, CHRU-Nancy, Université de Lorraine, Nancy, F-54000 France*

^c *Université de Lorraine, INSERM, U1254 IADI, F-54000 Nancy, France*

¹ Kamal Jouad and Emilien Mengel contributed equally to this work.

*Corresponding authors. Université de Lorraine, CNRS, L2CM, F-54000 Nancy, France. E-mail addresses: nadia.pellegrini@univ-lorraine.fr (N. Pellegrini Moïse), sandrine.langle@univ-lorraine.fr (S. Lamandé-Langle).

Abstract

The combination of positron emission tomography (PET)/photoacoustic imaging (PAI)/fluorescence imaging (FLI) for diagnosis allows to exploit the strengths and overcome the weaknesses of each modality. In this context, dyes displaying photophysical properties for both fluorescence and photoacoustic imaging in the near infra-red (NIR) window are ideal to maximize their signal-to-noise ratio. Herein, were synthesized a series of new meso-*O*-alkyl cyanine-7 derivatives, and the derivative bearing an azide was coupled to a highly functionalized *C*-glycosyl platform resulting in an imaging probe which exhibited both high molar absorptivity and fluorescence quantum yield (>15%), excellent characteristics for FLI and for PAI. Successfully radiolabeled with fluorine-18 *via* a [¹⁸F]F-C bond, this probe additionally allowed PET imaging. Altogether, these results revealed the multimodal PET/PAI/FLI imaging potential of this probe based on meso-*O*-alkyl heptamethine cyanine. Moreover, a late-stage CuAAC coupling with two model peptides c(RGDfK) was successfully performed to demonstrate the feasibility and the versatility of the vector conjugation step, foreshadowing of the expected targeting possibilities of this original platform for efficient disease diagnosis by multimodal imaging.

Keyword: Meso-*O*-alkyl cyanine-7, Fluorescence, Photoacoustic, PET, Multimodal imaging

1. Introduction

35 The combination of positron emission tomography (PET)/photoacoustic imaging
36 (PAI)/fluorescence imaging (FLI) for diagnosis allows to exploit the strengths and overcome
37 the weaknesses of each modality in terms of spatial resolution, detection sensitivity and
38 penetrability. PET is an imaging modality that utilizes radionuclide detection, and thus
39 requires a radioisotope. Fluorine-18 is an ideal isotope for PET imaging due to the [¹⁸F]F-C
40 covalent bond formation, its high molar activity and its suitable half-life ($t_{1/2} = 109.8$ min) for
41 permitting further chemical functionalization with vectors, ideally those with fast
42 biodistribution such as peptides.[1] This technique provides a high detection sensitivity (sub-
43 nanomolar range) without depth limitation, but has limited spatial resolution (1 to 5 mm
44 depending on the scanner).[2] FLI and PAI are two widely used and rapidly evolving optical
45 techniques for diagnosis and preclinical development that both take advantage of competitive
46 relaxation pathways occurring in a single photoactive dye, emissive and non-radiative
47 relaxation respectively. Thus, the lower the fluorescence quantum yield, the higher the
48 photothermal conversion in PAI. FLI is a well-established technique that provides high spatial
49 resolution of tens of nm and detection sensitivity in the nanomolar range. However, achieving
50 high-contrast imaging *in vivo* is challenging due to the scattering and reabsorption of
51 excitation and emission light, as well as interferences with intrinsic tissue fluorescence; these
52 physical hurdles therefore limit the depth of light penetration and the sensitivity due to low
53 signal-to-noise ratio.[3] To overcome these limitations, fluorophores with an
54 absorption/emission range in the NIR spectral window are commonly used and permit an
55 enhanced signal-to-noise ratio. Far reaching beyond imaging applications, FLI is also a key
56 technique for precise imaging-guided surgery.[4] On the other hand, PAI is a fast, inexpensive
57 and non-ionizing technique that has a sensitivity in the tens of nanomolar.[5,6] While PAI is
58 limited to the field of view of an organ, it is gaining popularity in preclinical development due
59 to its low scattering and deep penetrability of the signal, together with an optical spatial
60 resolution down to tens of microns, thus making it relevant for *in vivo* explorations.[7]
61 Altogether, combination of these three modalities will grant a well-balanced and realistic
62 diagnosis approach with high potential for future clinical translation using: 1) PET imaging
63 for a whole-body diagnosis, 2) PAI for a more localized organ imaging with enhanced
64 resolution and 3) FLI for both fluorescent-guided surgery and *ex vivo* histopathology.
65 Thus, a challenging goal in this research field is the design of photoactive dyes displaying
66 appropriate photophysical properties for concomitant use in both FLI and PAI. This dye must
67 display a fluorescence quantum yield and brightness sufficient for detecting their fluorescence
68 emission in the NIR by FLI, while simultaneously promoting thermal relaxation from the

69 excited state *via* non-radiative pathways, for an intense PA signal. Among fluorescent dyes,
70 cyanines have found extensive use in imaging applications.[8] Heptamethine cyanine
71 (cyanine-7, Cy7) derivatives are particularly attractive for biomedical use due to their
72 excellent biodegradability and biocompatibility. Moreover, their fluorescence excitation and
73 emission in the NIR-I window, and high brightness resulting from their high molar extinction
74 coefficient [9] makes them well-suited for imaging with high resolution and signal-to-noise
75 ratio during *in vivo* FLI and PAI.[7] This stronger absorption coefficient ($\epsilon > 200k$) in the NIR
76 region makes cyanines-7 more appealing for optical imaging than other dyes such as
77 BODIPYs or rhodamines. Their photophysical characteristics and their stability can be
78 modulated by modifying the heteroatom linked to the meso-position of Cy7 dyes.[9-11]
79 Meso-*O*-alkyl Cy7 derivatives, scarcely described in the literature,[12-16] indeed demonstrate
80 superior stability when compared to their -*N*-alkyl, -*S*-alkyl, or -*O*-aryl counterparts.[10,12]
81 Overall, Cy7 display the appropriate photophysical balance for performing in both FLI and
82 PAI using a single entity.

83 For such multimodal imaging, a major breakthrough in the field is the design of
84 monomolecular imaging agents, which enable the use of complementary molecular imaging
85 modalities with a single biodistribution profile.[17] While the monomolecular approaches for
86 the combination of either PET/FLI or PAI/FLI are well-established,[18,19] monomolecular
87 central cores that are competent in these three complementary imaging modalities
88 (PET/PAI/FLI) are scarce. To the best of our knowledge, only one example of a
89 monomolecular multimodal imaging agent that combined PET/PAI/FLI modalities is
90 described.[20] Going further toward functionalization of a monomolecular imaging agent
91 bearing a fluorescent/photoacoustic dye and a radioisotope, with an appropriate biological
92 vector for targeting remains a synthetical challenge. Yet, to successfully achieve it, we have
93 recently proved the advantage of a *C*-glycosyl platform that offers multifunctionalities for
94 selective introduction of the different entities at specific positions.[21,22]

95 In this study, we present a synthetic strategy for obtaining a multimodal PET/PAI/FLI
96 imaging probe based on a monomolecular approach. To achieve this, we first extended the
97 elegant *N*- to *O*-transposition reaction developed by Schnermann *et al.* to access novel meso-
98 *O*-alkyl cyanine derivatives for achieving both high stability and appropriate photophysical
99 properties for PAI and FLI. The meso-*O*-alkyl cyanine derivatives were designed with
100 functional groups for further straightforward conjugation, notably to a highly functionalized
101 *C*-glycosyl platform.[21,22] ^{18}F -radiolabelling by [^{18}F]F-C bond formation was successfully
102 performed, leading to a multimodal imaging probe. Finally, we proved the possibility to

103 introduce bioactive vectors, notably RGD peptide derivatives that are typically used as model
104 for targeting $\alpha_v\beta_3$ integrins, to afford a unique multimodal conjugate which fluorescent and
105 photoacoustic properties were fully evaluated.

106

107 2. Experimental section

108 2.1. General information

109 This section is summarized in the ESI. Compounds **1**[12], **14** to **24**[21,23], and **29**[21] were
110 prepared according to previously described methods (see ESI). Physico-chemical
111 characterization of meso-*N*-alkyl derivatives are described in the ESI.

112

113 2.2. General *N*- to *O*- transposition procedure

114 To a solution of electrophile carboxylic acid (0.36 mmol, 4.0 eq.) and DIPEA (15 μ L, 0.09
115 mmol, 1.0 eq.) in freshly distilled dichloromethane (3.5 mL) was added EDC (69 mg, 0.36
116 mmol, 4.0 eq.) at room temperature under inert atmosphere. The solution was stirred for 10
117 min, then compound **1** (65 mg, 0.09 mmol) was added. The reaction was heated to 40 °C in a
118 sealed tube for 18 hours, until the mixture's color changed from dark blue to green. The
119 reaction mixture was quenched with brine (10 mL), extracted with dichloromethane (2 \times 10
120 mL), and dried over MgSO₄. The solvent was removed under *vacuum* and the green residue
121 was purified by silica gel chromatography (0 to 5% MeOH/DCM) affording meso-*O*-alkyl
122 (green solid) and meso-*N*-alkyl (blue solid) cyanine derivatives.

123 2.2.1 Compound **2**. Yield: 72%; green solid; Mp = 97°C. ¹H NMR (400 MHz, CDCl₃)
124 compound exists as a mixture of two rotamers, major rotamer is designated by * and minor by
125 δ : δ 1.05 (t, 6H, $J_{4,5} = 7.5$ Hz, H-5), 1.37-1.45 (m, 2H, H-13), 1.55-1.67 (m, 4H, H-12, H-14),
126 1.69 (s, 12H, CH₃), 1.84-1.94 (m, 6H, H-7, H-4), 2.12 (app qt, 2H, $J_{9,8} = J_{9,10} = 6.5$ Hz, H-9),
127 2.30-2.42 (m, 2H, H-11), 2.57 (bt, 4H, $J = 6.0$ Hz, H-6), 3.02 (s, 3H, N-CH₃ δ), 3.11 (s, 3H, N-
128 CH₃*), 3.25 (t, 2H, $J = 7.0$ Hz, H-15), 3.64 (t, 2H, $J = 7.5$ Hz, H-10*), 3.69 (t, 2H, $J = 7.5$ Hz,
129 H-10 δ), 3.99-4.08 (m, 6H, H-8*, H-3), 4.11 (t, 2H, $J = 7.2$ Hz, H-8 δ), 6.00 (d, 2H, $J = 13.5$
130 Hz, H-1'* , H-7'*), 6.03 (d, 2H, $J = 13.5$ Hz, H-1' δ , H-7' δ), 7.09 (d, 2H, $J = 7.5$ Hz, HAr), 7.20
131 (t, 2H, $J = 7.5$ Hz, HAr), 7.32-7.40 (m, 4H, HAr), 8.00 (d, 2H, $J = 13.5$ Hz, H-2' δ , H-6' δ),
132 8.04 (d, 2H, $J = 13.5$ Hz, H-2'* , H-6'*). ¹³C NMR (100.6 MHz, CDCl₃): δ 11.8 (2C-5), 20.8
133 (2C-4), 21.1 (C-7), 24.6 (C-12 δ), 24.7 (C-12*), 24.8 (2C-6), 26.6 (C-13*), 26.7 (C-13 δ), 28.5
134 (4CH₃*), 28.6 (4CH₃ δ), 28.8 (C-9*), 28.9 (C-9 δ), 29.0 (C-14), 33.4 (C-11), 33.8 (N-CH₃ δ), 36.2
135 (N-CH₃*), 45.1 (C-10*), 46.0 (2C-3), 46.1 (C-10 δ), 49.0 (2C-2 δ), 49.1 (2C-2*), 51.3 (C-15 δ),

136 51.4 (C-15^δ), 75.0 (C-8^δ), 76.0 (C-8^{*}), 99.5 (C-1^{'*} and C-7^{'*}), 99.8 (C-1^{'δ} and C-7^{'δ}), 110.6
137 (2CAr^{*}), 110.7 (2CAr^δ), 122.3 (2CAr^δ), 122.4 (2CAr^{*}), 123.4 (C-3^{'*} and C-5^{'*}), 123.5 (C-3^{'δ}
138 and C-5^{'δ}), 125.0 (2CAr^{*}), 125.0 (2CAr^δ), 128.8 (2CAr^{*}), 128.9 (2CAr^δ), 140.6 (C-2^{'δ} and C-
139 6^{'δ}), 140.8 (C-2^{'*} and C-6^{'*}), 141.0 (2CqAr), 142.5 (2CqAr), 170.9 (C-4^{'δ}), 171.4 (C-4^{'*}),
140 171.5 (2C-1^δ), 171.5 (2C-1^{*}), 172.7 (C=O^δ), 173.0 (C=O^{*}). HRMS (ESI): [M⁺] calcd for
141 [C₄₆H₆₃N₆O₂⁺] 731.5007, found 731.5002. IR ($\bar{\nu}$ (cm⁻¹)): 2964, 2928, 2872, 2092, 1726, 1639,
142 1554, 1508, 1452, 1431, 1394, 13667, 1274, 1259, 1165, 929.

143 2.2.2. Compound **4**. Yield: 76%; green viscous oil; ¹H NMR (400 MHz, CDCl₃) compound
144 exists as a mixture of two rotamers, major rotamer is designated by * and minor by ^δ: δ 1.03
145 (t, 6H, $J_{4,5} = 7.5$ Hz, H-5), 1.57-1.68 (m, 4H, H-12, H-13), 1.68 (s, 12H, CH₃), 1.81-1.92 (m,
146 6H, H-7, H-4), 2.19 (app qt, 2H, $J_{9,8} = J_{9,10} = 6.5$ Hz, H-9), 2.36 (t, 2H, $J = 7.0$ Hz, H-11^{*}),
147 2.43 (t, 2H, $J = 7.0$ Hz, H-11^δ), 2.55 (bt, 4H, $J = 6.0$ Hz, H-6), 3.01 (s, 3H, N-CH₃^δ), 3.11 (s,
148 3H, N-CH₃^{*}), 3.27 (t, 2H, $J = 7.0$ Hz, H-14), 3.63 (t, 2H, $J = 7.5$ Hz, H-10^{*}), 3.67 (t, 2H, $J =$
149 7.5 Hz, H-10^δ), 3.98-4.06 (m, 6H, H-8^{*}, H-3), 4.10 (t, 2H, $J = 7.2$ Hz, H-8^δ), 5.98 (d, 2H, $J =$
150 13.5 Hz, H-1^{'*}, H-7^{'*}), 6.01 (d, 2H, $J = 13.5$ Hz, H-1^{'δ}, H-7^{'δ}), 7.09 (d, 2H, $J = 7.5$ Hz, HAr),
151 7.19 (t, 2H, $J = 7.5$ Hz, HAr), 7.30-7.40 (m, 4H, HAr), 8.00 (d, 2H, $J = 13.5$ Hz, H-2^{'δ}, H-
152 6^{'δ}), 8.03 (d, 2H, $J = 13.5$ Hz, H-2^{'*}, H-6^{'*}). ¹³C NMR (100.6 MHz, CDCl₃): δ 11.7 (2C-5),
153 20.7 (2C-4), 21.0 (C-7), 22.2 (C-12), 24.7 (2C-6), 28.4 (4CH₃^{*}), 28.5 (4CH₃^δ), 28.6 (C-13),
154 29.0 (C-9), 32.9 (C-11), 33.7 (N-CH₃^δ), 36.2 (N-CH₃^{*}), 45.1 (C-10^{*}), 45.9 (2C-3), 47.0 (C-
155 10^δ), 48.9 (2C-2^δ), 49.0 (2C-2^{*}), 51.1 (C-14^δ), 51.3 (C-14^{*}), 75.9 (C-8^δ), 75.9 (C-8^{*}), 99.4 (C-
156 1^{'*} and C-7^{'*}), 99.7 (C-1^{'δ} and C-7^{'δ}), 110.5 (2CAr^{*}), 110.6 (2CAr^δ), 122.3 (2CAr^δ), 122.4
157 (2CAr^{*}), 123.3 (C-3^{'*} and C-5^{'*}), 123.4 (C-3^{'δ} and C-5^{'δ}), 124.9 (2CAr^{*}), 125.0 (2CAr^δ),
158 128.7 (2CAr^{*}), 128.8 (2CAr^δ), 140.6 (C-2^{'δ} and C-6^{'δ}), 140.7 (C-2^{'*} and C-6^{'*}), 141.0
159 (2CqAr), 142.4 (2CqAr), 171.3 (C-4^{'δ}), 171.4 (C-4^{'*}), 171.5 (2C-1), 172.6 (C=O). HRMS
160 (ESI): [M⁺] calcd for [C₄₅H₆₁N₆O₂⁺] 717.4851, found 717.4856. IR ($\bar{\nu}$ (cm⁻¹)): 2919.83,
161 2090.50, 1554.10, 1505.68, 1365.84, 1247.99, 1150.00, 1038.94, 920.04, 793.81, 511.76.

162 2.2.3. Compound **6**. Yield: 79%; green solid; Mp = 90°C. ¹H NMR (400 MHz, CD₃CN)
163 compound exists as a mixture of two rotamers, major rotamer is designated by * and minor by
164 ^δ: δ 1.00 (t, 6H, $J_{4,5} = 7.5$ Hz, H-5), 1.60-1.71 (m, 2H, H-12), 1.67 (s, 12H, CH₃), 1.76-1.87
165 (m, 6H, H-7, H-4), 2.02-2.10 (m, 2H, H-13), 2.17 (app qt, 2H, $J_{9,8} = J_{9,10} = 7.0$ Hz, H-9^{*}), 2.21
166 (app qt, 2H, $J_{9,8} = J_{9,10} = 7.0$ Hz, H-9^δ), 2.29 (t, 2H, $J_{11,12} = 7.5$ Hz, H-11^{*}), 2.38 (t, 2H, $J_{11,12}$
167 = 7.5 Hz, H-11^δ), 2.56-2.63 (m, 4H, H-6), 2.94 (s, 3H, N-CH₃^δ), 3.02 (s, 3H, N-CH₃^{*}), 3.57

168 (t, 2H, H-10*), 3.62 (t, 2H, H-10^δ), 3.98-4.06 (m, 6H, H-8, H-3), 4.89-5.02 (m, 2H, H-15),
169 5.76-5.87 (m, 1H, H-14), 6.09 (d, 2H, $J = 14.0$ Hz, H-1', H-7''), 6.10 (d, 2H, $J = 14.0$ Hz, H-
170 1'^δ, H-7'^δ), 7.20-7.27 (m, 4H, HAr), 7.38 (t, 2H, $J = 7.5$ Hz, HAr), 7.46 (d, 2H, $J = 7.5$ Hz,
171 HAr), 8.07 (bd, 2H, $J = 14.0$ Hz, H-2',^δ H-6',^δ). ¹³C NMR (100.6 MHz, CD₃CN): δ 11.6
172 (2C-5), 21.3 (2C-4), 22.0 (C-7), 25.0 (2C-12*), 25.2 (2C-6), 25.4 (2C-12^δ), 28.5 (4CH₃), 29.7
173 (C-9*), 30.6 (C-9^δ), 32.8 (C-11[□]), 33.1 (C-11*), 33.6 (N-CH₃^δ), 34.0 (C-13*), 34.0 (C-13^δ),
174 35.9 (N-CH₃*), 45.3 (C-10*), 46.3 (2C-3), 47.5 (C-10^δ), 49.9 (2C-2^δ), 49.9 (2C-2*), 75.8 (C-
175 8^δ), 76.8 (C-8*), 100.3 (C-1'* and C-7''), 100.4 (C-1'^δ and C-7'^δ), 111.8 (2CAr*), 111.9
176 (2CAr^δ), 115.3 (C-15*), 115.4 (C-15^δ), 123.2 (2CAr), 123.7 (C-3'^δ and C-5'^δ), 123.7 (C-3'*
177 and C-5'*), 125.0 (2CAr*), 125.1 (2CAr^δ), 129.5 (2CAr), 139.5 (C-14^δ), 139.6 (C-14*), 141.5
178 (C-2'^δ and C-6'^δ), 141.7 (C-2'* and C-6'*), 142.0 (2CqAr), 143.7 (2CqAr), 171.3 (C-4'^δ),
179 171.7 (C-4'*), 172.8 (2C-1), 173.0 (C=O^δ), 173.4 (C=O*). HRMS (ESI): [M⁺] calcd for
180 [C₄₆H₆₂N₃O₂⁺] 688.4837, found 688.4832. IR ($\bar{\nu}$ (cm⁻¹)): 3406, 2965, 2927, 1637, 1556,
181 1508, 1452, 1396, 1369, 1251, 1165, 1091, 1047, 1001, 929.

182 2.2.4. Compound **8**. Yield: 50%; green solid; Mp = 74°C. ¹H NMR (400 MHz, CDCl₃)
183 compound exists as a mixture of two rotamers, major rotamer is designated by * and minor by
184 ^δ: δ 1.01 (t, 6H, $J_{4,5} = 7.5$ Hz, H-5), 1.66 (s, 12H, CH₃), 1.75-1.90 (m, 9H, H-12, H-7, H-4, H-
185 15), 2.17 (app qt, 2H, $J_{9,8} = J_{9,10} = 6.5$ Hz, H-9), 2.23 (td, 2H, $J_{13,12} = 7.5$ Hz, $J_{13,15} = 2.5$ Hz,
186 H-13), 2.43 (t, 2H, $J_{11,12} = 7.5$ Hz, H-11*), 2.51 (t, 2H, $J_{11,12} = 7.5$ Hz, H-11^δ), 2.54 (bt, 4H,
187 $J_{6,7} = 6.0$ Hz, H-6), 3.00 (s, 3H, N-CH₃^δ), 3.10 (s, 3H, N-CH₃*), 3.61 (t, 2H, $J_{10,9} = 7.5$ Hz, H-
188 10*), 3.67 (t, 2H, $J_{10,9} = 7.5$ Hz, H-10^δ), 3.99-4.06 (m, 2H, H-8), 4.01 (t, 4H, $J_{4,3} = 7.5$ Hz, H-
189 3), 5.96 (d, 2H, $J = 14.0$ Hz, H-1', H-7''), 5.99 (d, 2H, $J = 14.0$ Hz, H-1'^δ, H-7'^δ), 7.08 (d,
190 2H, $J = 7.5$ Hz, HAr), 7.17 (t, 2H, $J = 7.5$ Hz, HAr), 7.29-7.36 (m, 4H, HAr), 7.98 (d, 2H, $J =$
191 14.0 Hz, H-2'^δ, H-6'^δ), 8.01 (d, 2H, $J = 14.0$ Hz, H-2'* , H-6'*). ¹³C NMR (100.6 MHz,
192 CDCl₃): δ 11.7 (2C-5), 17.9 (C-13^δ), 18.0 (C-13*), 20.7 (2C-4), 20.9 (C-7), 23.7 (C-12^δ), 24.0
193 (C-12*), 24.6 (2C-6), 28.4 (4CH₃*), 28.4 (4CH₃^δ), 28.9 (C-9), 31.8 (C-11*), 32.8 (C-11^δ), 33.7
194 (N-CH₃^δ), 36.0 (N-CH₃*), 45.0 (C-10*), 45.9 (2C-3), 46.0 (C-10^δ), 48.9 (2C-2^δ), 48.9 (2C-2*),
195 69.0 (C-15*), 69.1 (C-15^δ), 74.9 (C-8^δ), 75.8 (C-8*), 83.5 (C-14^δ), 83.8 (C-14*), 99.3 (C-1'*
196 and C-7''), 99.6 (C-1'^δ and C-7'^δ), 110.5 (2CAr*), 110.6 (2CAr^δ), 122.2 (2CAr^δ), 122.3
197 (2CAr*), 123.2 (C-3'* and C-5'*), 123.3 (C-3'^δ and C-5'^δ), 124.8 (2CAr*), 124.9 (2CAr^δ),
198 128.7 (2CAr*), 128.8 (2CAr^δ), 140.5 (C-2'^δ and C-6'^δ), 140.6 (C-2'* and C-6'*), 140.9
199 (2CqAr), 142.3 (2CqAr), 170.7 (C-4'^δ), 171.3 (C-4'*), 171.3 (2C-1^δ), 171.4 (2C-1*), 172.3

200 (C=O*) 175.4 (C=O δ). HRMS (ESI): [M⁺] calcd for [C₄₆H₆₀N₃O₂⁺] 686.4680, found
201 686.4708. IR ($\bar{\nu}$ (cm⁻¹)): 2962, 2924, 2872, 2183, 1734, 1647, 1554, 1450, 1363, 1275, 995.

202 2.2.5. Compound **10**. Yield: 39%; green viscous oil; ¹H NMR (400 MHz, CDCl₃) compound
203 exists as a mixture of two rotamers, major rotamer is designated by * and minor by δ : δ 1.06
204 (t, 6H, $J_{4,5} = 7.5$ Hz, H-5), 1.71 (s, 12H, CH₃), 1.85-1.95 (m, 6H, H-7, H-4), 1.94 (t, 1H, $J_{14,13}$
205 = 2.5 Hz, H-14), 2.22 (app qt, 2H, $J_{9,8} = J_{9,10} = 7.0$ Hz, H-9*), 2.26 (app qt, 2H, $J_{9,8} = J_{9,10} =$
206 7.0 Hz, H-9 δ), 2.49-2.54 (m, 2H, H-12), 2.56-2.67 (m, 6H, H-11, H-6), 3.06 (s, 3H, N-CH₃ δ),
207 3.14 (s, 3H, N-CH₃*), 3.67 (t, 2H, $J_{10,9} = 7.5$ Hz, H-10*), 3.69 (t, 2H, $J_{10,9} = 7.5$ Hz, H-10 δ),
208 4.02-4.15 (m, 6H, H-8, H-3), 6.02 (d, 2H, $J = 14.0$ Hz, H-1'*), H-7'*), 6.07 (d, 2H, $J = 14.0$
209 Hz, H-1' δ , H-7' δ), 7.09 (d, 2H, $J = 7.5$ Hz, HAr), 7.21 (t, 2H, $J = 7.5$ Hz, HAr), 7.33-7.40 (m,
210 4H, HAr), 8.02 (d, 2H, $J = 14.0$ Hz, H-2' δ , H-6' δ), 8.05 (d, 2H, $J = 14.0$ Hz, H-2'*), H-6'*). ¹³C
211 NMR (100.6 MHz, CDCl₃): δ 11.8 (2C-5* δ), 14.6 (C-12*), 14.8 (C-12 δ), 20.9 (2C-4), 21.1 (C-
212 7), 24.8 (2C-6), 28.5 (4CH₃), 28.6 (C-9*), 29.1 (C-9 δ), 32.6 (C-11), 33.9 (N-CH₃ δ), 36.1 (N-
213 CH₃*), 45.3 (C-10*), 46.1 (2C-3), 46.2 (C-10 δ), 49.1 (2C-2 δ), 49.1 (2C-2*), 68.8 (C-14), 76.0
214 (C-8), 83.7 (C-13), 99.7 (C-1'* and C-7'*), 100.0 (C-1' δ and C-7' δ), 110.6 (2CAr*), 110.7
215 (2CAr δ), 122.4 (2CAr δ), 122.5 (2CAr*), 123.7 (C-3'* and C-5'*), 123.8 (C-3' δ and C-5' δ),
216 125.0 (2CAr*), 125.1 (2CAr δ), 128.8 (2CAr*), 128.9 (2CAr δ), 140.6 (C-2' δ and C-6' δ), 140.9
217 (C-2'* and C-6'*), 141.1 (2CqAr), 142.6 (2CqAr), 170.6 (C-4' δ), 171.1 (C-4'*), 171.4 (2C-1 δ),
218 171.5 (2C-1*), 171.5 (C=O). HRMS (ESI): [M⁺] calcd for [C₄₅H₅₈N₃O₂⁺] 672.4524, found
219 672.4499. IR ($\bar{\nu}$ (cm⁻¹)): 2964, 2920, 2872, 2189, 1734, 1647, 1554, 1452, 1363, 1151, 916.

220

221 2.3. Synthesis of compounds **25** and **26**.

222 To a solution of **10** or **11** (0.042 mmol) in ACN (1 mL), 12 mg of **2** (0.046 mmol, 1.1 eq.), 40
223 μ L of sodium ascorbate (1M in water, 0.042 mmol), and 14 μ L of copper (II) acetate (0.3 M
224 in water, 0.038 mmol, 0.9 eq.) were added, and the mixture was stirred at room temperature
225 for 24 h. The mixture was diluted with EtOAc and washed with brine (3 \times 10 ml). The organic
226 solvent was dried over MgSO₄ and removed under *vacuum*. The crude product was purified
227 using a flash chromatography on silica gel (eluent: DCM/MeOH 100/0 to 90/10) to afford
228 compound **25** or **26**.

229 2.3.1. Compound **25**. Yield: 50%. green viscous oil. ¹H NMR (400 MHz, CDCl₃) compound
230 exists as a mixture of two rotamers, major rotamer is designated by * and minor by δ : δ 0.98-
231 1.05 (m, 48H, H-27, Si-isopropyl), 1.34 (app qt, 2H, $J_{17,18} = J_{17,16} = 6.5$ Hz, H-17), 1.58-1.65
232 (m, 2H, H-18), 1.66 (s, 12H, CH₃), 1.80-1.96 (m, 10H, H-2, H-16, H-26, H-29), 2.11-2.21 (m,

233 2H, H-21), 2.29 (t, 2H, $J_{19,18} = 7.5$ Hz, H-19^{*}), 2.35 (t, 2H, $J_{19,18} = 7.5$ Hz, H-19^δ), 2.54 (bt,
234 4H, $J_{28,29} = 6.0$ Hz, H-28), 2.98 (s, 3H, N-CH₃^δ), 3.06 (s, 3H, N-CH₃^{*}), 3.56-3.64 (m, 4H, H-
235 20, H-1), 3.95-4.10 (m, 7H, H-25, H-22, H-6), 4.13-4.21 (m, 1H, H-3), 4.21-4.32 (m, 4H, H-
236 4, H-5, H-15), 4.31 (s, 2H, H-8 or H-11), 4.33-4.46 (m, 1H, H-7a), 4.40 (s, 2H, H-8 or H-11),
237 4.40-4.57 (m, 1H, H-7b), 4.52-4.60 (m, 2H, H-14), 5.98 (d, 2H, $J = 14.0$ Hz, H-1^{'*}, H-7^{'*}),
238 6.02 (d, 2H, $J = 14.0$ Hz, H-1^{'δ}, H-7^{'δ}), 7.07 (d, 2H, $J = 8.0$ Hz, HAr), 7.18 (t, 2H, $J = 8.0$ Hz,
239 HAr), 7.30-7.37 (m, 4H, HAr), 7.56 (s, 1H, H-triazole), 7.98 (d, 2H, $J = 14.0$ Hz, H-2^{'δ}, H-
240 6^{'δ}), 8.01 (d, 2H, $J = 14.0$ Hz, H-2^{'*}, H-6^{'*}). ¹³C NMR (CDCl₃, 100.6 MHz): δ (ppm) = 11.1
241 (3C, Si-CH-(CH₃)₂), 11.1 (3C, Si-CH-(CH₃)₂), 11.7 (2C-27), 18.5 (6C, Si-CH-(CH₃)₂), 18.6
242 (6C, Si-CH-(CH₃)₂), 20.8 (2C-26), 21.0 (C-29), 24.3 (C-18), 24.6 (2C-28), 26.3 (C-17), 28.4
243 (4CH₃), 28.9 (C-21^{*}), 29.7(C-21^δ), 30.1 (C-2), 30.2 (C-16), 32.7 (C-19^δ), 33.2 (C-19^{*}), 33.6
244 (N-CH₃^δ), 35.8 (N-CH₃^{*}), 45.1 (C-20), 45.8 (2C-25), 49.0 (2C-24), 50.1 (C-15), 58.5 (C-8 or
245 C-11), 59.0 (C-8 or C-11), 64.6 (C-14), 67.4 (C-1), 74.8 (C-22^δ), 75.8 (C-22^{*}, C-4), 77.6 (C-
246 3), 77.8 (d, $J_{C5-F} = 6.0$ Hz, C-5), 78.5 (d, $J_{C6-F} = 18.0$ Hz, C-6), 82.8 (d, $J_{C7-F} = 173.0$ Hz, C-
247 7), 88.6 (C-10 or C-13), 88.8 (C-10 or C-13), 99.4 (C-1^{'*}, C-7^{'*}), 99.7 (C-1^{'δ}, C-7^{'δ}), 103.2
248 (C-9 or C-12), 103.0 (C-9 or C-12), 110.5 (2CAr^{*}), 110.6 (2CAr^δ), 122.3 (2CAr^{*}), 122.4 (CH-
249 triazole), 122.5 (2CAr^δ), 123.3 (C-3^{'*}, C-5^{'*}), 123.4 (C-3^{'δ}, C-5^{'δ}), 125.0 (2CAr^{*}), 125.1
250 (2CAr^δ), 128.8 (2CAr^{*}), 128.8 (2CAr^δ), 140.6 (C-2^{'δ}, C-6^{'δ}), 140.7 (2CqAr), 140.9 (C-2^{'*}, C-
251 6^{'*}), 142.4 (2CqAr), 145.4 (Cq-triazole), 170.8 (2C-23^δ), 171.3 (2C-23^{*}), 171.5 (C=O), 172.3
252 (C-4^{'δ}), 172.7 (C-4^{'*}). ¹⁹F NMR (CD₃CN, 376 MHz): δ -231.0 (td, $J_{F,H-7} = 47.0$ Hz, $J_{F,H-6} =$
253 27.0 Hz). HRMS (ESI): [M+H]²⁺ calcd for [C₈₀H₁₂₃FN₆O₆Si₂]²⁺ 669.4508, found 669.4530.
254 IR ($\bar{\nu}$ (cm⁻¹)): 3387, 3005, 2958, 2939, 2864, 2169, 1637, 1556, 1508, 1394, 1365, 1228,
255 1163, 1151, 1085, 1043, 929.

256 2.3.2. Compound **26**. Yield: 95%. green viscous oil. ¹H NMR (400 MHz, CDCl₃) compound
257 exists as a mixture of two rotamers, major rotamer is designated by * and minor by δ: δ 0.98-
258 1.07 (m, 57H, H-27, Si-isopropyl, Si-tert-butyl), 1.32-1.40 (m, 2H, H-17), 1.61-1.68 (m, 2H,
259 H-18), 1.70 (s, 12H, CH₃), 1.75-1.89 (m, 10H, H-2, H-16, H-26, H-29), 2.20 (app qt, 2H,
260 $J_{21,20} = J_{21,22} = 7.5$ Hz, H-21^{*}), 2.23 (app qt, 2H, $J_{21,20} = J_{21,22} = 7.5$ Hz, H-21^δ), 2.31 (t, 2H,
261 $J_{19,18} = 7.5$ Hz, H-19^{*}), 2.39 (t, 2H, $J_{19,18} = 7.5$ Hz, H-19^δ), 2.58 (bt, 4H, $J = 6.0$ Hz, H-28),
262 3.00 (s, 3H, N-CH₃^δ), 3.09 (s, 3H, N-CH₃^{*}), 3.59-3.77 (m, 6H, H-20, H-1, H-7), 3.97-4.08 (m,
263 7H, H-25, H-22, H-6), 4.13-4.33 (m, 7H, H-3, H-4, H-5, H-15, H-8 or H-11), 4.41-4.60 (m,
264 4H, H-8 or H-11, H-14), 5.99 (d, 2H, $J = 13.5$ Hz, H-1^{'*}, H-7^{'*}), 6.01 (d, 2H, $J = 13.5$ Hz, H-

265 1^δ, H-7^δ), 7.08 (d, 2H, $J = 7.5$ Hz, HAr), 7.20 (t, 2H, $J = 7.5$ Hz, HAr), 7.31-7.42 (m, 10H,
266 HAr), 7.46 (s, 1H, H-triazole), 7.62-7.69 (m, 4H, HAr), 8.01 (d, 2H, $J = 13.5$ Hz, H-2^δ, H-
267 6^δ), 8.05 (d, 2H, $J = 13.5$ Hz, H-2^{*}, H-6^{*}). ¹³C NMR (CDCl₃, 100.6 MHz): δ (ppm) = 11.2
268 (3C, Si-CH-(CH₃)₂), 11.2 (3C, Si-CH-(CH₃)₂), 11.6 (2C-27), 18.6 (6C, Si-CH-(CH₃)₂), 18.6
269 (6C, Si-CH-(CH₃)₂), 19.3 (C, Si-C), 20.8 (2C-26), 21.1 (C-29), 24.3 (C-18), 24.7 (2C-28),
270 26.9 (C-17), 26.9 (3C, Si-C(CH₃)₃), 28.5 (2CH₃), 28.6 (2CH₃), 29.0 (C-21), 30.2 (C-2), 30.3
271 (C-16), 32.9 (C-19^δ), 33.3 (C-19^{*}), 33.7 (N-CH₃^δ), 36.2 (N-CH₃^{*}), 45.1 (C-20), 45.9 (2C-25),
272 49.0 (2C-24), 50.1 (C-15), 58.5 (C-8 or C-11), 59.0 (C-8 or C-11), 64.6 (C-14), 64.6 (C-7),
273 67.8 (C-1), 76.0 (C-22), 77.0 (C-3 and C-4), 79.0 (C-5), 81.2 (C-6), 87.9 (C-10 and C-13),
274 99.5 (C-1^{*}, C-7^{*}), 99.8 (C-1^δ, C-7^δ), 103.1 (C-9 or C-12), 103.4 (C-9 or C-12), 110.5
275 (2CAr), 122.2 (CH-triazole), 122.3 (2CAr^δ), 122.4 (2CAr^{*}), 123.4 (C-3^{*}, C-5^{*}), 123.5 (C-
276 3^δ, C-5^δ), 125.0 (2CAr), 127.7 (2CAr), 127.7 (2CAr), 128.8 (2CAr), 129.7 (CAr), 129.7
277 (CAr), 133.4 (CqAr), 133.5 (CqAr), 135.6 (2CAr), 135.7 (2CAr), 140.6 (C-2^δ, C-6^δ), 140.7
278 (2CqAr), 141.1 (C-2^{*}, C-6^{*}), 142.2 (2CqAr), 145.6 (Cq-triazole), 171.5 (2C-23), 171.5 (C-
279 4^γ), 172.7 (C=O). HRMS (ESI): [M+H]²⁺ calcd for [C₉₆H₁₄₂N₆O₇Si₃]²⁺ 787.5118, found
280 787.5082. IR ($\bar{\nu}$ (cm⁻¹)): 2928, 2891, 2862, 2359, 2341, 1637, 1554, 1506, 1452, 1431, 1396,
281 1367, 1263, 1226, 1165, 1153, 1089, 999, 920.

282

283 2.4. Synthesis of compounds **27** and **28**.

284 To a solution of **25** or **26** (0.023 mmol) in THF (1 mL), 54 μ L of tetrabutylammonium
285 fluoride (1 M in THF, 0.054 mmol, 2.4 eq.) was added at 0 °C under an inert atmosphere, and
286 the mixture was stirred at 0 °C for 1h or overnight for **25** and **26** respectively. The organic
287 solvent was removed under reduced pressure, and the residue was solubilized in CH₂Cl₂ (10
288 mL). The organic layer was washed with 0.1 M HCl solution (5 mL) and with brine until pH
289 = 7. The organic layer was dried over MgSO₄, and the solvent was removed under vacuum.
290 The crude product was purified using a flash chromatography on silica gel (eluent:
291 DCM/MeOH 100/0 to 90/10) to afford compound **27** or **28**.

292 2.4.1. Compound **27**. Yield: 75%. green foam. ¹H NMR (400 MHz, CDCl₃) compound exists
293 as a mixture of two rotamers, major rotamer is designated by * and minor by ^δ: δ 1.04 (t, 6H,
294 $J_{26,27} = 7.5$ Hz, H-27), 1.36 (app qt, 2H, $J_{17,18} = J_{17,16} = 6.5$ Hz, H-17), 1.60-1.67 (m, 2H, H-
295 18), 1.69 (s, 12H, CH₃), 1.82-1.97 (m, 10H, H-2, H-16, H-26, H-29), 2.15-2.22 (m, 2H, H-
296 21), 2.31 (t, 2H, $J_{19,18} = 7.5$ Hz, H-19^{*}), 2.37 (t, 2H, $J_{19,18} = 7.5$ Hz, H-19^δ), 2.45 (t, 1H, $J =$
297 2.5 Hz, H-10 or H-13), 2.50 (t, 1H, $J = 2.5$ Hz, H-10 or H-13), 2.51-2.61 (m, 4H, H-28), 3.00

298 (s, 3H, N-CH₃^δ), 3.08 (s, 3H, N-CH₃^{*}), 3.58-3.66 (m, 4H, H-20, H-1), 3.96-4.11 (m, 7H, H-
 299 25, H-22, H-6), 4.15-4.21 (m, 3H, H-3, H-4, H-5), 4.27 (d, 2H, H-8 or H-11), 4.35 (t, 2H,
 300 $J_{15,16} = 7.5$ Hz, H-15), 4.38 (d, 2H, H-8 or H-11), 4.38-4.51 (m, 1H, H-7a), 4.51-4.63 (m, 1H,
 301 H-7b), 4.55-4.61 (m, 2H, H-14), 6.03 (bs, 2H, H-1'^{δ,*}, H-7'^{δ,*}), 7.09 (bd, 2H, $J = 8.0$ Hz,
 302 HAr), 7.21 (bs, 2H, HAr), 7.31-7.40 (m, 4H, HAr), 7.67 (s, 1H, H-triazole), 8.02 (bs, 2H, H-
 303 2'^{*δ}, H-6'^{*δ}). ¹³C NMR (CDCl₃, 100.6 MHz): δ (ppm) = 11.8 (2C-27), 20.8 (2C-26), 21.1 (C-
 304 29), 24.4 (C-18), 24.7 (2C-28), 26.3 (C-17), 28.5 (4CH₃), 29.0 (C-21^{*}), 29.5 (C-21^δ), 29.8 (C-
 305 2), 30.3 (C-16), 32.8 (C-19^δ), 33.3 (C-19^{*}), 33.7 (N-CH₃^δ), 35.9 (N-CH₃^{*}), 45.1 (C-20), 45.9
 306 (2C-25), 49.0 (2C-24), 50.2 (C-15), 58.4 (C-8 or C-11), 58.6 (C-8 or C-11), 64.5 (C-14), 67.3
 307 (C-1), 74.9 (C-22^δ), 75.0 (C-22^{*}), 75.6 (C-4), 75.9 (C-10 or C-13), 76.5 (C-10 or C-13), 77.7
 308 (C-3), 78.3 (d, $J_{C6-F} = 18.0$ Hz, C-6), 79.1 (d, $J_{C5-F} = 6.0$ Hz, C-5), 79.3 (C-9 or C-12), 79.9
 309 (C-9 or C-12), 82.7 (d, $J_{C7-F} = 173.0$ Hz, C-7), 99.5 (C-1'^{*}, C-7'^{*}), 99.8 (C-1'^δ, C-7'^δ), 110.6
 310 (2CAr^{*}), 110.6 (2CAr^δ), 122.4 (2CAr^{*}), 122.8 (CH-triazole), 123.5 (2CAr^δ), 123.4 (C-3'^{*}, C-
 311 5'^{*}), 123.5 (C-3'^δ, C-5'^δ), 125.1 (2CAr^{*}), 125.1 (2CAr^δ), 128.8 (2CAr^{*}), 128.9 (2CAr^δ), 140.6
 312 (C-2'^δ, C-6'^δ), 140.8 (2CqAr), 141.0 (C-2'^{*}, C-6'^{*}), 142.5 (2CqAr), 145.2 (Cq-triazole), 170.8
 313 (2C-23^δ), 171.4 (2C-23^{*}), 171.5 (C=O), 172.5 (C-4'^δ), 172.8 (C-4'^{*}). ¹⁹F NMR (CD₃CN, 376
 314 MHz): δ -232.0 (td, $J_{F,H-7} = 49.0$ Hz, $J_{F,H-6} = 28.0$ Hz). HRMS (ESI): [M+H]²⁺ calcd for
 315 [C₆₂H₈₃FN₆O₆]²⁺ 513.3174, found 513.3175. IR ($\bar{\nu}$ (cm⁻¹)): 3286, 3005, 2987, 2924, 2856,
 316 2318, 1735, 1635, 1556, 1508, 1452, 1396, 1363, 1311, 1224, 1163, 1082, 927.

317 2.4.2. Compound **28**. Yield: 82%. green foam. ¹H NMR (400 MHz, CD₃CN) compound exists
 318 as a mixture of two rotamers, major rotamer is designated by * and minor by ^δ: δ 1.01 (t, 6H,
 319 $J_{26,27} = 7.5$ Hz, H-27), 1.26-1.33 (m, 2H, H-17), 1.51-1.64 (m, 2H, H-18), 1.68 (s, 12H, CH₃),
 320 1.76-1.90 (m, 10H, H-2, H-16, H-26, H-29), 2.13-2.24 (m, 2H, H-21), 2.28 (t, 2H, $J_{19,18} = 7.5$
 321 Hz, H-19^{*}), 2.37 (t, 2H, $J_{19,18} = 7.5$ Hz, H-19^δ), 2.59 (bt, 4H, $J = 6.0$ Hz, H-28), 2.72 (t, 1H, J
 322 = 2.5 Hz, H-10 or H-13), 2.75 (t, 1H, $J = 2.5$ Hz, H-10 or H-13), 2.93 (s, 3H, N-CH₃^δ), 3.01
 323 (s, 3H, N-CH₃^{*}), 3.34-3.64 (m, 6H, H-20, H-1, H-7), 3.72-3.77 (m, 1H, H-6), 3.97-4.07 (m,
 324 8H, H-25, H-22, H-4, H-3), 4.08-4.13 (m, 1H, H-5), 4.22-4.36 (m, 6H, H-15, H-8, H-11),
 325 4.41-4.53 (m, 2H, H-14), 6.07 (d, 2H, $J = 13.5$ Hz, H-1'^{*}, H-7'^{*}), 6.09 (d, 2H, $J = 13.5$ Hz, H-
 326 1'^δ, H-7'^δ), 7.21-7.27 (m, 4H, HAr), 7.39 (t, 2H, $J = 7.5$ Hz, HAr), 7.47 (d, 2H, $J = 7.5$ Hz,
 327 HAr), 7.74 (s, 1H, H-triazole), 8.07 (d, 2H, $J = 13.5$ Hz, H-2'^δ, H-6'^δ), 8.08 (d, 2H, $J = 13.5$
 328 Hz, H-2'^{*}, H-6'^{*}). ¹³C NMR (CD₃CN, 100.6 MHz): δ 11.6 (2C-27), 21.3 (2C-26), 22.0 (C-
 329 29), 25.0 (C-18), 25.1 (2C-28), 26.8 (C-17), 28.5 (2CH₃), 28.6 (2CH₃), 29.7 (C-21^{*}), 30.0 (C-
 330 21^δ), 30.3 (C-2), 30.8 (C-16), 32.6 (C-19^δ), 33.3 (N-CH₃^δ), 33.6 (C-19^{*}), 35.9 (N-CH₃^{*}), 45.3

331 (C-20^{*}), 46.3 (2C-25), 47.5 (C-20^δ), 49.9 (2C-24), 50.6 (C-15), 58.7 (C-8 or C-11), 59.1 (C-8
332 or C-11), 62.8 (C-7), 64.7 (C-14), 67.7 (C-1), 75.7 (C-10 or C-13), 76.0 (C-22), 76.9 (C-3),
333 77.9 (C-9 or C-12), 78.6 (C-4), 80.8 (C-5), 81.0 (C-9 or C-12), 81.1 (C-10 or C-13), 81.4 (C-
334 6), 100.2 (C-1^{'*}, C-7^{'*}), 100.3 (C-1^{'δ}, C-7^{'δ}), 111.7 (CAr), 111.8 (CAr), 123.2 (C-3^{'*}, C-5^{'*}),
335 123.3 (C-3^{'δ}, C-5^{'δ}), 123.7 (2CAr^δ), 123.7 (2CAr^{*}), 124.0 (CH-triazole), 125.6 (2CAr^{*}), 125.7
336 (2CAr^δ), 129.5 (2CAr), 141.5 (C-2^{'δ}, C-6^{'δ}), 141.7 (C-2^{'*}, C-6^{'*}), 142.0 (2CqAr), 143.7
337 (2CqAr), 145.7 (Cq-triazole), 171.4 (C-4^{'δ}), 171.8 (C-4^{'*}), 172.8 (2C-23), 173.4 (C=O).
338 HRMS (ESI): [M+H]²⁺ calcd for [C₆₂H₈₄N₆O₇]²⁺ 512.3195, found 512.3216. IR ($\bar{\nu}$ (cm⁻¹):
339 2929, 2863, 2350, 2335, 1637, 1554, 1506, 1452, 1431, 1396, 1367, 1263, 1226, 1165, 1153,
340 1089, 999, 920.

341

342 2.5. Synthesis of compound **30**

343 To a solution of **27** (6.3 mg, 5.5 μ mol, 1.0 eq.) in a mixture of DMF/H₂O (1/1 v/v) (1 mL), 23
344 mg of **29** (27.3 μ mol, 4.2 eq.), 27 μ L of copper (II) sulphate (1 M in water, 27 μ mol, 3.0 eq.),
345 and 55 μ L of sodium ascorbate (1 M in water, 54.6 μ mol, 10 eq.) were added, and the mixture
346 was stirred at 40 °C for 24 h. The solvent was removed under *vacuum* and the crude product
347 was purified using size-exclusion chromatography on Sephadex LH20 in methanol/H₂O (1/1
348 v/v) to afford compound **30** in 15% yield as a green solid after freeze drying. HRMS (ESI):
349 [M]³⁺ calcd for [C₁₃₈H₂₀₄FN₃₀O₃₀]³⁺ 926.8442, found 926.8414.

350

351 2.6. Synthesis of compound **32**

352 To a solution of **31** (18 mg, 0.016 mmol) in freshly distilled CH₂Cl₂ (1.5 mL), 14 μ L of
353 DIPEA (0.079 mmol, 5.0 equiv.) and 11 mg of methanesulfonic anhydride (0.063 mmol, 4.0
354 equiv.) were added under inert atmosphere. The mixture was stirred for 16 hours at room
355 temperature. The solution was diluted in CH₂Cl₂ (20 mL) and the organic layer was washed
356 with saturated NH₄Cl (10 mL) and brine. The organic layer was dried over MgSO₄ and the
357 solvent was removed under *vacuum*. The crude product was purified by flash chromatography
358 on silica gel (eluent: DCM/MeOH 4/6) to afford compound **32** in 60% yield as a green foam.
359 ¹H NMR (400 MHz, CD₃CN) compound exists as a mixture of two rotamers, major rotamer is
360 designated by * and minor by ^δ: δ 1.01 (t, 6H, $J_{26,27} = 7.5$ Hz, H-27), 1.28-1.33 (m, 2H, H-17),
361 1.51-1.64 (m, 2H, H-18), 1.68 (s, 12H, CH₃), 1.76-1.90 (m, 10H, H-2, H-16, H-26, H-29),
362 2.14-2.23 (m, 2H, H-21), 2.28 (t, 2H, $J_{19,18} = 7.5$ Hz, H-19^{*}), 2.37 (t, 2H, $J_{19,18} = 7.5$ Hz, H-
363 19^δ), 2.59 (bt, 4H, $J = 6.0$ Hz, H-28), 2.73 (t, 1H, $J = 2.5$ Hz, H-10 or H-13), 2.79 (t, 1H, $J =$

364 2.5 Hz, H-10 or H-13), 2.94 (s, 3H, N-CH₃^δ), 3.01 (s, 3H, N-CH₃^{*}), 3.03 (s, 3H, CH₃-Ms),
365 3.46-3.66 (m, 4H, H-20, *H-1*), 3.92-4.12 (m, 10H, H-25, H-22, *H-4*, H-3, H-6, H-5), 4.18-4.39
366 (m, 8H, *H-15*, *H-8*, *H-11*, H-7), 4.42-4.50 (m, 2H, H-14), 6.07 (d, 2H, *J* = 13.5 Hz, H-1'^{*}, H-
367 7'^{*}), 6.09 (d, 2H, *J* = 13.5 Hz, H-1'^δ, H-7'^δ), 7.20-7.27 (m, 4H, HAr), 7.39 (t, 2H, *J* = 7.5 Hz,
368 HAr), 7.47 (d, 2H, *J* = 7.5 Hz, HAr), 7.70 (s, 1H, H-triazole), 8.07 (d, 2H, *J* = 13.5 Hz, H-2'^δ,
369 H-6'^δ), 8.09 (d, 2H, *J* = 13.5 Hz, H-2'^{*}, H-6'^{*}). ¹³C NMR (CD₃CN, 100.6 MHz): δ 11.6 (2C-
370 27), 21.3 (2C-26), 22.0 (C-29), 25.1 (C-18), 25.2 (2C-28), 26.9 (C-17), 28.6 (4CH₃), 29.7 (C-
371 21^{*}), 30.3 (C-21^δ), 30.6 (C-2), 30.8 (C-16), 32.6 (C-19^δ), 33.6 (C-19^{*}), 34.3 (N-CH₃^δ), 35.9
372 (N-CH₃^{*}), 37.7 (CH₃-Ms), 45.3 (C-20^{*}), 46.3 (2C-25), 47.5 (C-20^δ), 49.9 (C-15), 50.6 (2C-
373 24), 59.0 (C-8 or C-11), 59.3 (C-8 or C-11), 64.8 (C-14), 67.6 (C-1), 71.0 (C-7), 75.9 (C-10 or
374 C-13), 76.5 (C-22), 76.9 (C-6), 77.8 (C-9 or C-12), 78.1 (C-4), 78.5 (C-3), 80.6 (C-5), 80.8
375 (C-9 or C-12), 81.0 (C-10 or C-13), 100.3 (C-1'^{*}, C-7'^{*}), 100.3 (C-1'^δ, C-7'^δ), 111.7 (CAr),
376 111.8 (CAr), 123.2 (C-3'^{*}, C-5'^{*}), 123.3 (C-3'^δ, C-5'^δ), 123.7 (2CAr^δ), 123.7 (2CAr^{*}), 124.0
377 (CH-triazole), 125.7 (2CAr^{*}), 125.7 (2CAr^δ), 129.5 (2CAr), 141.5 (C-2'^δ, C-6'^δ), 141.8 (C-2'^{*},
378 C-6'^{*}), 142.0 (2CqAr), 143.7 (2CqAr), 145.6 (Cq-triazole), 171.4 (C-4'^δ), 171.8 (C-4'^{*}),
379 172.9 (2C-23), 173.3 (C=O). ¹⁹F NMR (CD₃CN, 376 MHz): δ -79.5. HRMS (ESI): [M+H]²⁺
380 calcd for [C₆₃H₈₆N₆O₉S]²⁺ 551.3083, found 551.3065. IR ($\bar{\nu}$ (cm⁻¹)): 2930, 2870, 2340, 2330,
381 1637, 1554, 1506, 1452, 1431, 1396, 1367, 1263, 1226, 1165, 1153, 1089, 998.

382

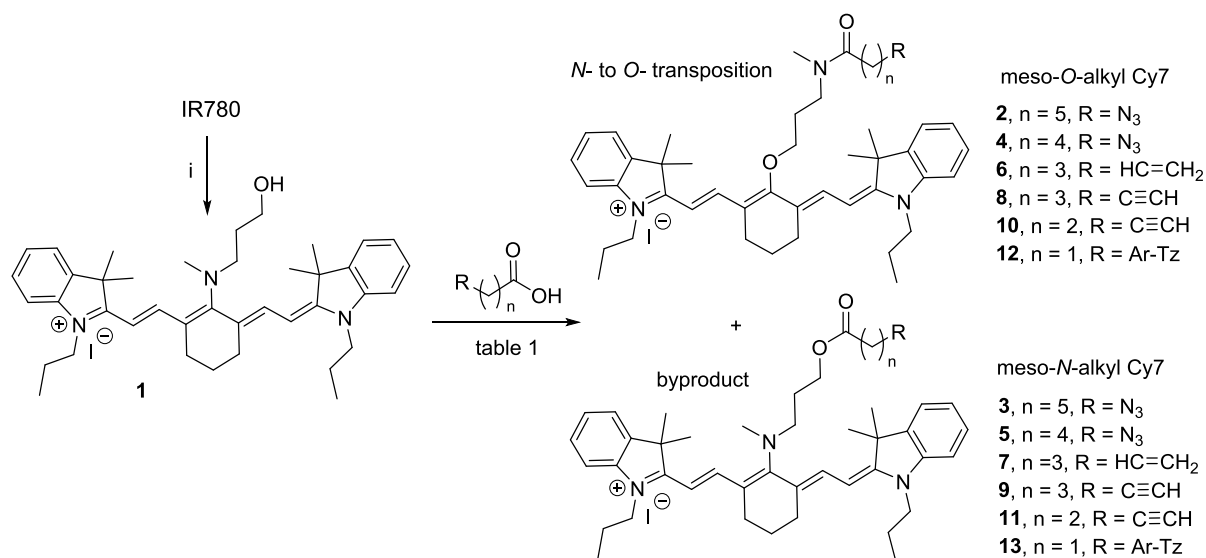
383 3. Results and discussion

384 3.1. Synthesis of novel meso-*O*-alkyl Cy7 derivatives ready for click coupling

385 The nature of the atom (Cl, N, S, O) on the meso-position of Cy7 affects the stability and
386 photophysical properties of the dye and, therefore, its potential as imaging agent.[9-11] While
387 *N*-alkyl, *-S*-alkyl or *-O*-aryl Cy7 are the most described in the literature, the meso-*O*-alkyl
388 Cy7 derivatives are known to exhibit greater stability.[10,12] Although direct nucleophilic
389 substitution on the meso-Cl of the commercial Cy7 derivative (IR780) with amine, thiol or
390 phenol derivatives is straightforward, it is far more challenging with alkyl alcohols and
391 explains the lower number of reports concerning meso-*O*-alkyl Cy7 compounds.[10]
392 Schnermann *et al.* reported an efficient method to access these compounds: meso-*N*-alkyl Cy7
393 derivatives obtained by nucleophilic substitution of the meso-Cl of IR780 are then
394 transformed into meso-*O*-alkyl Cy7 compounds *via* a *N*- to *O*-transposition with electrophiles,
395 notably exemplified with carboxylic acids activated *in situ*.[12,13]. We have extended this
396 reaction with various carboxylic acids to provide new meso-*O*-alkyl Cy7 derivatives bearing

397 functional groups suitable for copper-catalyzed alkyne-azide cycloaddition (CuAAC),[24]
398 inverse electron demand Diels–Alder (IEDDA),[25] and thiol-ene reactions.[26]
399 The compound **1** was prepared by the reaction of commercial IR780 and 3-
400 (methylamino)propan-1-ol in acetonitrile (Scheme 1).[12] This key intermediate **1** was then
401 submitted to the *N*- to *O*-transposition under various conditions with different carboxylic
402 acids bearing an azide, an alkyne or an alkene (Scheme 1). Based on the report of
403 Schnermann *et al.*, the first assay was performed using 6-azidohexanoic acid with HATU (7
404 equiv.) as activating agent and DIPEA (8 equiv.) in DMF at 35°C during 18h (Table 1, entry
405 1). Transposed meso-*O*-alkyl compound **2** was obtained in poor yield (13%), whereas the
406 meso-*N*-alkyl byproduct **3**, resulting from *O*-acylation, was isolated in 53% yield.
407 Schnermann *et al.* reported the formation of these type of *O*-acylated compounds using an
408 electrophile such as AcCl.[12] The structure of compound **3** was confirmed by ¹H and ¹³C
409 NMR spectra and mass spectrometry. Of note, for meso-*O*-alkyl Cy7 **2**, two rotamers formed
410 by the amide function were clearly recognizable on ¹H NMR spectra, which contrastingly was
411 not observed for the meso-*N*-alkyl **3**. Compounds **2** (green powder) and **3** (blue viscous oil)
412 were separated by column chromatography (See ESI Fig S4, for optical spectra). EDC was
413 then used for preactivation (4 equiv) in a second experiment with DIPEA (1 equiv.) in DCM
414 at 40°C for 18h (Table 1, entry 2). The meso-*O*-alkyl Cy7 **2** was then successfully obtained in
415 66% yield along with meso-*N*-alkyl Cy7 **3** in only 12% yield. In the same conditions, another
416 attempt was performed in a sealed tube (entry 3), which allowed to reach 82% yield for the
417 desired meso-*O*-alkyl Cy7 **2**, the formation of **3** being limited to 8%. While optimizing this
418 protocol, different parameters have been changed: the number of equivalents of electrophile
419 (entry 4), the reaction temperature (entry 5) and also the use of another activating agent
420 (PyBop, entry 6), that yet failed at exceeding previous yield. The best protocol found in entry
421 3, was then successfully implemented with 5-azidopentanoic acid leading exclusively to
422 meso-*O*-alkyl **4** in 76% yield. Other functionalized electrophiles were tested in these optimal
423 conditions, hex-5-enoic acid and hex-5-ynoic acid (Table 1, entries 8 and 9), which led to
424 meso-*O*-alkyl compounds **6** and **8** in 79 and 50% respectively. We can note that meso-*N*-alkyl
425 byproduct **9** was also produced in 5% yield, whereas no meso-*N*-alkyl derivative was isolated
426 when the reaction was performed with hex-5-enoic acid. In the case of pent-4-ynoic acid, the
427 predominant compound was the meso-*N*-alkyl Cy7 **11** obtained in 50% yield, the meso-*O*-
428 alkyl Cy7 **10** being nevertheless isolated in 39% (Table 1, entry 10). Finally, we attempted to
429 use a carboxylic acid displaying a tetrazine moiety for IEDDA conjugation (entry 11),

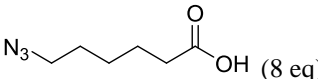
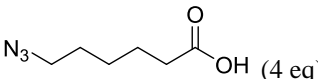
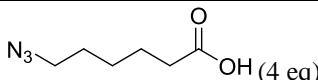
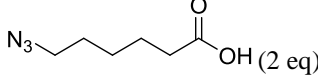
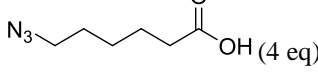
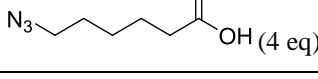
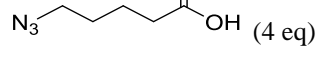
430 however no *N*- to *O*-transposition occurred, certainly due to the rigidity generated by the
 431 phenyl spacer. The meso-*N*-alkyl Cy7 **13** was the only compound formed in 81% yield.

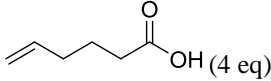
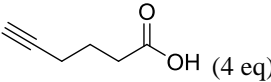
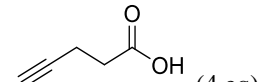
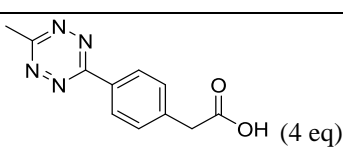


432
 433 Scheme 1. Reagents and conditions: i) 3-(methylamino)propan-1-ol, acetonitrile, rt, 15min,
 434 96%.

435

436 Table 1. Scope and limitation of *N*- to *O*- transposition reaction

Entry	Electrophile	Reaction conditions	Product, isolated yield	
			meso- <i>O</i> -alkyl Cy7	meso- <i>N</i> -alkyl Cy7
1	 (8 eq)	HATU (7 eq.), DIPEA (8 eq.), DMF, 35°C, 18h, round bottom flask	2 , 13%	3 , 53%
2	 (4 eq)	EDC (4eq), DIPEA (1eq), DCM, 40°C, 18h, round bottom flask	2 , 66%	3 , 12%
3	 (4 eq)	EDC (4eq), DIPEA (1eq), DCM, 40°C, 18h, sealed tube	2 , 82%	3 , 8%
4	 (2 eq)	EDC (4eq), DIPEA (1eq), DCM, 40°C, 18h, sealed tube	2 , 64%	3 , 7%
5	 (4 eq)	EDC (4eq), DIPEA (1eq), DCM, 50°C, 18h, sealed tube	2 , 66% ^a	3 , 6%
6	 (4 eq)	PyBop (2 eq), DIPEA (3 eq), rt, 20h, sealed tube	2 , 45%	3 , 20%
7	 (4 eq)	EDC (4eq), DIPEA (1eq), DCM, 40°C, 18h, sealed tube	4 , 76%	5 , traces

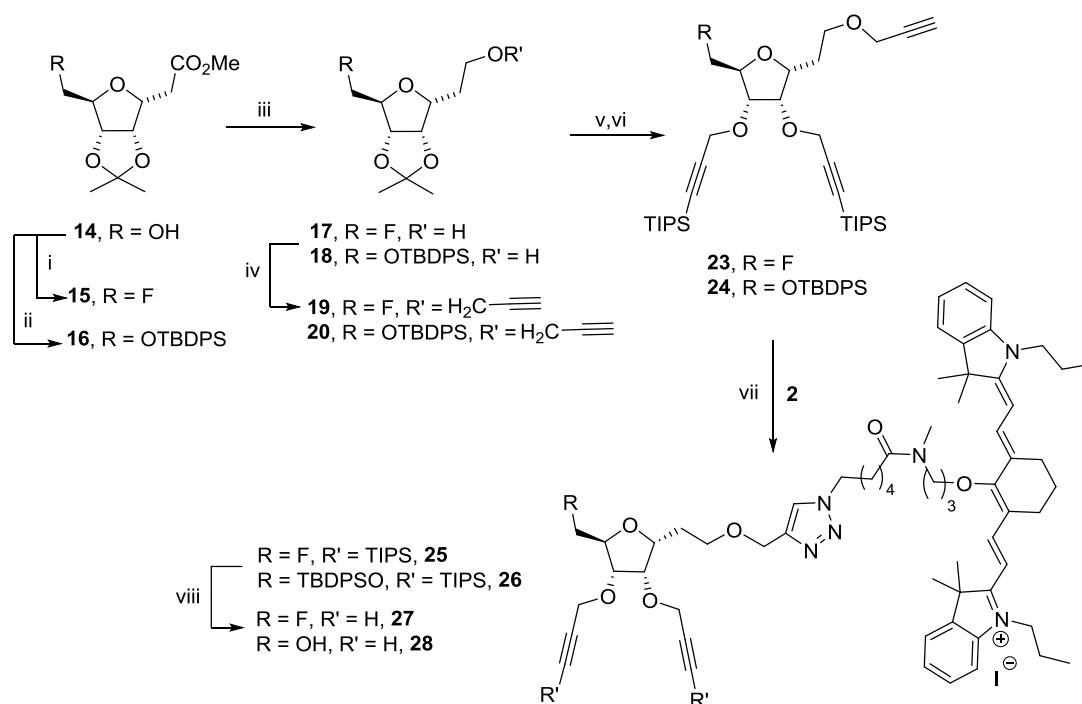
8		EDC (4eq), DIPEA (1eq), DCM, 40°C, 18h, sealed tube	6 , 79%	7 , 0%
9		EDC (4eq), DIPEA (1eq), DCM, 40°C, 18h, sealed tube	8 , 50%	9 , 5%
10		EDC (4eq), DIPEA (1eq), DCM, 40°C, 18h, sealed tube	10 , 39%	11 , 50%
11		EDC (4eq), DIPEA (1eq), DCM, 40°C, 18h, sealed tube	12 , 0%	13 , 81%

437 ^adegradation products was observed

438

439 3.2. Synthesis of the multimodal probe

440 Having in hand meso-*O*-alkyl derivatives ready for click coupling, we then focused on the
441 synthesis of the targeted multimodal PET/PAI/FLI imaging probe. To this end, we used a
442 properly functionalized *C*-glycosyl central platform for enabling the regioselective grafting of
443 both imaging and targeting entities. *C*-glycosyl compounds have a stable C-C bond on the
444 pseudo-anomeric carbon, making them resistant to enzymatic hydrolysis which is crucial for
445 *in vivo* applications.[27] We recently developed a clickable *C*-glycosyl scaffold, designed
446 with free and temporarily masked triple bonds which is ideal for their activation at the
447 appropriate synthetic step, thus allowing the sequential introduction of a fluorine atom *via*
448 nucleophilic substitution and also a fluorophore and targeting moieties via CuAAC.[21,22] A
449 similar multi-step synthetic strategy was used to access both the non-radioactive probe (with a
450 ¹⁹F) and the radiolabelling precursor bearing a leaving group required for subsequent ¹⁸F-
451 radiolabelling process. Briefly, compound **14** was synthesized as previously reported[28] and
452 further fluorinated with DAST or protected with a TBDPS (Scheme 2). The reduction of
453 methyl ester on compounds **15** and **16** followed by propargylation of the resulting alcohol led
454 to compounds **19** and **20** in high yields. In order to sequentially introduce by CuAAC first the
455 photoactive dye and then the targeting entities in a later stage, two TIPS-protected alkynes
456 were introduced after removal of the 4,5-isopropylidene protecting group. Ethers **23** and **24**
457 were obtained in 94% and 78% yields, respectively. The azido cyanine **2** was selected for
458 CuAAC coupling with alkyne **23** and **24**, resulting in the formation after purification by
459 column chromatography of cycloadducts **25** and **26** in 50% and 95% yields respectively. The
460 temporary TIPS and TBDPS protecting groups were then removed with tetrabutylammonium
461 fluoride, then providing compounds **27** and **28** in high yields.

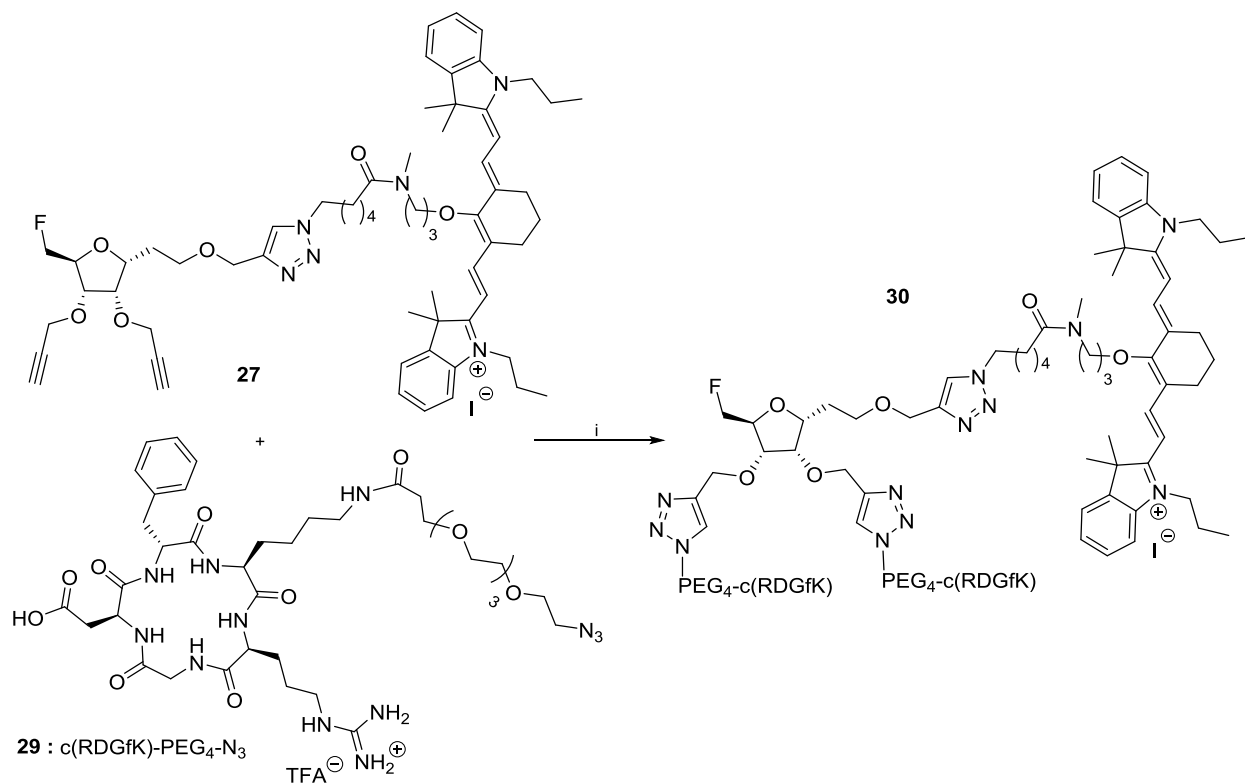


463
 464 Scheme 2. Reagents and conditions: i) DAST, diglyme, 0 °C to 110 °C, 2 h, 85%; ii)
 465 TBDPSCl, imidazole, DMF, 0 °C to rt, 16 h, 95%; iii) LiAlH₄, THF, 0 °C to rt, 2 h, **17**: 82%,
 466 **18**: 80%; iv) propargyl bromide, NaH, 0 °C to rt, 16 h, **19**: 95% in DMF, **20**: 70% in THF; v)
 467 TFA/H₂O, rt, 3 h, **21**: 84% or AcOH/H₂O, 80 °C, 4 h, **22**: 54%; vi) TIPS-propargyl bromide,
 468 NaH, 0 °C to rt, 5 h, **23**: 94% in DMF, **24**: 78% in THF. vii) Cu(OAc)₂ (0.1 equiv.), sodium
 469 ascorbate (0.2 equiv.), ACN/H₂O (1/1 v/v), 12 h, rt, **25**: 50%, **26**: 95%; viii) TBAF (1 M,
 470 THF), THF, 0 °C, 1 h or 0 °C to rt, 12 h, **27**: 75%, **28**: 82%.

471 472 3.3. Coupling of the probe with targeting entities

473 Conjugation with targeting vectors in the final step allows versatility in receptor targeting and
 474 therefore facilitates further change of vectors for their facile adaptation to imaging another
 475 biological target. Herein, the feasibility of CuAAC coupling with peptide vectors was
 476 demonstrated by reaction with a model peptide c(RGDfK), known for selectively binding to
 477 $\alpha_v\beta_3$ integrins and widely used as model for cancer diagnosis and tumor imaging.[29] A
 478 c(RGDfK) analog previously modified with an alkyne-PEG₄ **29**[21] selected to increase the
 479 hydrophilicity of the platform, was reacted with the photoactive probe **27**. This reaction took
 480 place at 40 °C during 24 h in a mixture of DMF/H₂O 1/1 using excess of copper(II) sulfate and
 481 sodium ascorbate (Scheme 3). Purification by steric exclusion gel filtration afforded the
 482 conjugate **30** in 15% yield after freeze drying. Importantly, because two vacant positions
 483 remain on the C-glycosyl platform, coupling with two c(RGDfK) peptides would provide

484 access to divalence which has been suggested as an attractive option to enhance targeting
485 efficiency.[21,22,30] This proof of concept with RGD derivatives thus paves the way for
486 peptide-divalent probes relevant for *in vivo* imaging applications.



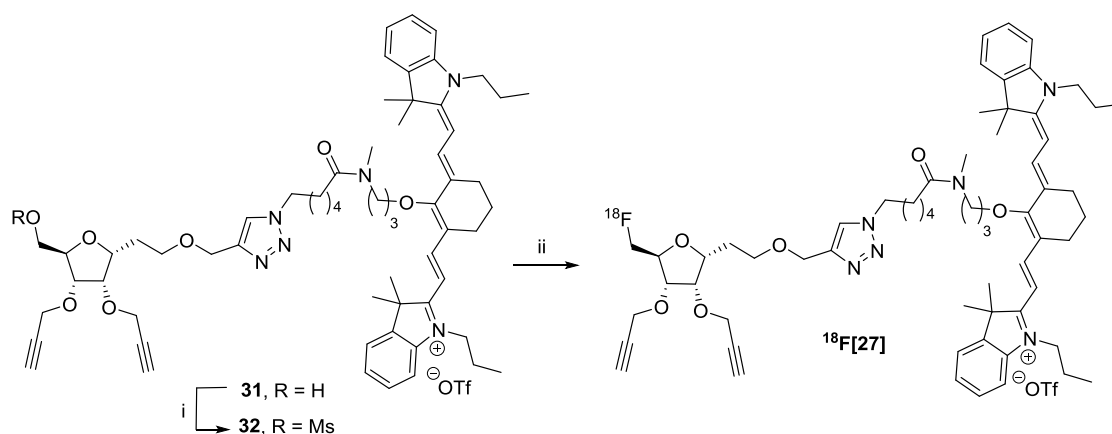
487
488

489 Scheme 3. Reagents and conditions: (i) CuSO₄ (3 equiv.), sodium ascorbate (10 equiv.),
490 DMF/H₂O 1/1 v/v, 40°C, 24 h, 15%.

491

492 3.4. Synthesis of radiolabelling precursor and ¹⁸F-radiolabelling

493 The synthesis of the radiolabelling precursor was then implemented. In this context, because
494 the iodide counter anion of cyanine **28** can compromise the subsequent ¹⁸F-fluorination by
495 competitive nucleophilic substitution, it was exchanged with a triflate anion (non-nucleophilic
496 anion). The anion metathesis of compound **28** was carried out using an Oasis[®] MCX cartridge
497 with a solution of silver triflate (0.2 M) to afford compound **31**. A leaving group was then
498 introduced to allow subsequent ¹⁸F-radiolabelling (Scheme 4). The reaction was carried out at
499 room temperature with methane sulfonic anhydride and DIPEA during 12 h and mesylated
500 compound **32** was obtained in 60% yield.



501
 502 Scheme 4. Reagents and conditions: i) Ms_2O , DIPEA, DCM, 0°C to rt, 12 h, 60%; ii)
 503 $\text{K}[^{18}\text{F}]\text{F-K}_{222}$, acetonitrile, 95°C , 15 min, 19%.

504
 505 The radiolabelling of mesylated precursor **32** with fluorine-18 was investigated using an
 506 AllInOne synthesizer. Building upon our previous successful radiosynthesis of a cyanine-5
 507 (Cy5) based probe *via* direct radiofluorination for formation of a $[^{18}\text{F}]\text{F-C}$ bond,^[21,22] the
 508 same conditions were employed herein, namely using the $\text{K}[^{18}\text{F}]\text{F-K}_{222}$ complex in
 509 acetonitrile at 95°C . Optimization of the reaction time (5, 10 and 15 min) showed that 15
 510 minutes provided the best yield. Analysis of the crude mixture by radio-HPLC showed the
 511 formation of $[^{18}\text{F}]\mathbf{27}$ with an incorporation yield of 19%, which is a good yield for this type of
 512 radiolabelling involving the formation of $[^{18}\text{F}]\text{F-C}$ bond. The structure of $[^{18}\text{F}]\mathbf{27}$ was
 513 confirmed by comparison with the non-radioactive compound **27**, both displaying identical
 514 retention times in HPLC (see ESI, Fig S2 and S3). We thus proved the successful extension of
 515 this radiofluorination approach from a Cy5-based probe to the more challenging Cy7-based
 516 compound. Automated peptide coupling on $[^{18}\text{F}]\mathbf{27}$ is currently in progress to perform
 517 preclinical PET imaging.

518
 519 3.5. Optical and photoacoustic properties

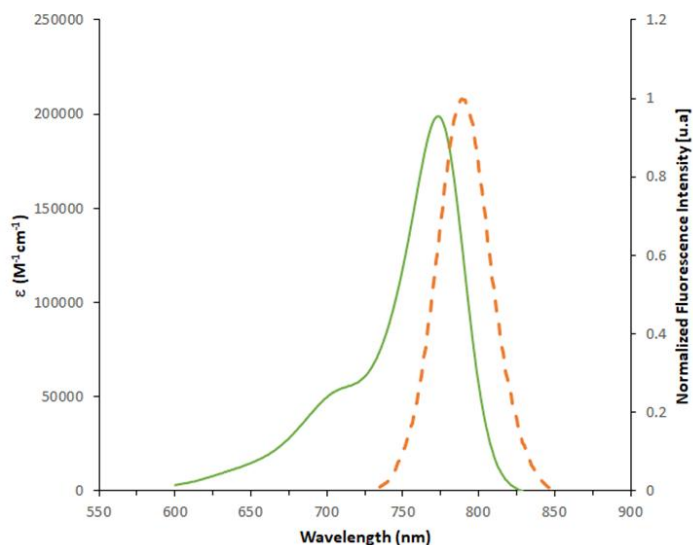
520 To explore the influence of functional groups on the photophysical characteristics of meso-*O*-
 521 alkyl heptamethine cyanines (Table 1), we studied the properties of the representative meso-
 522 *O*-alkyl Cy7 derivatives bearing an azide (compound **2**), an alkene (compound **6**), and an
 523 alkyne group (compound **8**). Moreover, the photophysical characteristics of the *C*-glycosyl
 524 central platform functionalized by the meso-*O*-alkyl Cy7 derivative **2** (compound **27**) were
 525 also evaluated. Thus, the optical properties (absorption and emission wavelengths, relative
 526 fluorescence quantum yield Φ_{fluo} and molecular brightness *B*) of compounds **2**, **6** and **8**, as
 527 well as the multimodal imaging probe **27** were characterized by steady-state one photon

528 absorption/emission measurements in DMSO and compared to commercial IR780 and ICG
 529 (Table 2, Fig 1). More precisely, the cyanine derivatives **2**, **6** and **8** display one major
 530 absorption band with a maximum located at 772 nm and an emission band characterized by a
 531 small Stokes shift ($\Delta\lambda = 13\text{--}18$ nm, Table 2). All studied derivatives exhibited high molar
 532 absorption coefficients in DMSO that are comparable with the parent dye IR780 (Table 2).
 533 The fluorescence quantum yields are relatively high ($\Phi_{\text{fluo}} >15\%$) and do not vary
 534 significantly among derivatives of meso-*O*-alkyl Cy7, thus no apparent effect of the
 535 functional group was observed on their photophysical properties. Introduction of the *C*-
 536 glycosyl platform by CuAAC on compound **2** leading to the probe **27** only had a small effect
 537 on photophysical properties. Hypsochromically shifted absorption and emission profiles were
 538 observed with sufficiently high molar absorptivity and improved fluorescence quantum yield
 539 relative to the IR780 reference, indicating that **27** has excellent characteristics for optical
 540 imaging purpose. Moreover, meso-*O*-alkyl cyanines compare favorably with the well-
 541 established indocyanine green (ICG, Table 2) that is approved by both the FDA and EMA as
 542 an intraoperative fluorescent agent, and granted NIR photoactivation albeit with a moderate
 543 Stokes shift.

544 Table 2. Selected photophysical properties of meso-*O*-alkyl Cy7 derivatives, IR780 and ICG measured in
 545 DMSO.
 546

Compound	λ_{abs} (nm)	λ_{em} (nm)	Stokes shift $\Delta\nu$ (cm^{-1}) / $\Delta\lambda$ (nm)	ϵ ($\text{M}^{-1} \text{cm}^{-1}$)	$\Phi_{\text{fluo}}^{[b]}$ (%)	$B^{[c]}$ ($\text{M}^{-1} \text{cm}^{-1}$)
2	773	786	214 / 13	226 600	23	52 100
6	773	786	214 / 13	250 000	15	37 500
8	773	789	260 / 16	214 000	22	47 100
27	772	790	295 / 18	202 400	19	38 500
IR780	794	815	325 / 21	228 200	8 ^[a]	18 300
ICG	795 ^[d]	820 ^[d]	383 / 25	224 000 ^[d]	16.7 ^[d]	37 400

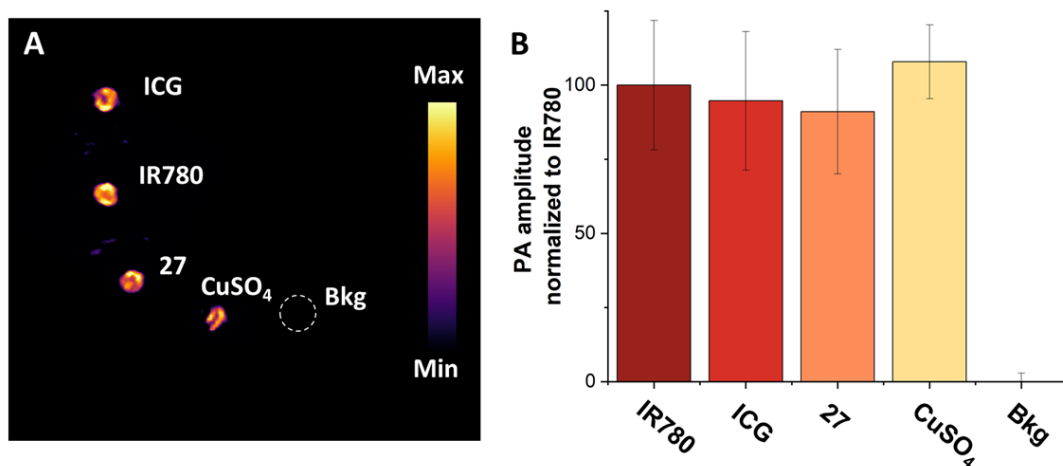
547 [a] relative to $\Phi_{\text{fluo}} = 8\%$ of IR780 in EtOH[31], [b] $\lambda_{\text{ex}} = 750$ nm, [c] Fluorescence brightness =
 548 $\epsilon \times \Phi_{\text{fluo}}$, [d] from reference [32]
 549



550
 551 Figure 1. Molar absorption coefficients (full line) and emission (dotted line) spectra recorded
 552 at 298 K for compound **27** in DMSO, $\lambda_{\text{ex}} = 750$ nm.

553
 554 Next, we performed phantom imaging to investigate the PA contrast produced by probe **27**.
 555 A photoacoustic tomograph using a curved transducer was operated as previously described
 556 [33] with selected samples loaded in PTFE tube and mounted on a rotating holder immersed
 557 into deionized water. Under NIR irradiation at its maximal absorbance wavelength, *i.e.* 772
 558 nm, compound **27** proved to display intense PA contrast (Figure 2). Its PA amplitude is found
 559 to linearly increase along to concentration (see ESI, Figure S5), which is expected due to its
 560 correlation with the agent's absorbance.[34-36] Of note, calibration of PA tomograph is a
 561 challenging task,[37] hence instead an internal standard is used for ensuring repeatability
 562 among imaging sessions and for accurate quantification of PA signal. CuSO_4 was selected as
 563 the internal standard because it absorbs between 650-1000 nm, showing an intense absorption
 564 at the selected wavelength of 772 nm, and neither suffers photobleaching nor
 565 photodegradation. Compound **27** displayed significant PA amplitude with a detection limit
 566 below the tens of micromolar (Figure S5), and its PA amplitude compared favorably with two
 567 well-established cyanine-7 derivatives, *i.e.* ICG and IR780 (Figure 2).

568
 569



570
 571 Figure 2. Phantom imaging in photoacoustic under irradiation at 772 nm of **27** and
 572 comparison to golden standards ICG and IR780, diluted in DMSO at 40 μ M. A)
 573 Representative PA image of the samples and B) comparison of their PA amplitude normalized
 574 to IR780.

575
 576 Because PA imaging relies on a photophysical process that is competitive with fluorescence,
 577 and both modalities are looked after herein, we aimed at reasonably boosting the fluorescence
 578 quantum yield of our dyes for achieving a greater signal-to-noise ratio in FLI, while
 579 maintaining sufficient PA amplitude. This balance between radiative and non-radiative
 580 deexcitation pathways is well demonstrated by weighting out the absorption properties (ϵ
 581 values at the irradiation wavelength) together with fluorescence properties (quantum yield of
 582 fluorescence) of IR780 and **27**. As previously shown in Table 2, *Cl*- to *O*-substitution of
 583 IR780 has an important impact on the Φ_{fluo} values (8% and 19% for IR780 and **27**,
 584 respectively) hence boosting the emissive desexcitation pathway. These results show that **27**
 585 displayed a higher fluorescence quantum yield together with a high PA contrast that is
 586 comparable to IR780 at the same molar concentration. Both **27** and IR780 displayed
 587 comparable PA amplitude at 772 nm probably because of the higher absorptivity of **27** at this
 588 selected wavelength than IR780 (143 000 and 202 400 $\text{M}^{-1}\text{cm}^{-1}$ for IR780 and **27**,
 589 respectively).

590
 591 The development of sophisticated probes competent for multimodal imaging is a daunting
 592 challenge and further illustrated by the limited number of multimodal PET/PAI/FLI imaging
 593 agents described in the literature.[20]. This task encompasses multiple challenges, including
 594 synthesis, radiosynthesis, and the careful selection of a dye suitable for both FLI and PAI
 595 applications. For probing the possibility of overcoming this synthetic challenge, we

596 previously, devised a synthetic strategy that permitted the introduction onto a C-glycosidic
597 platform of a fluorine-18 for forming a stable [¹⁸F]F-C bond together with a Cy5 dye.[21]
598 Building upon this successful synthetic proof of concept, we aimed herein at overcoming the
599 photophysical limitations of Cy5 for optical imaging by adapting this protocol to the more
600 suitable NIR active cyanine-7 while expanding the landscape of this synthetic approach.
601 Consequently, we selected herein the challenging meso-*O*-alkyl Cy7 derivatives that are more
602 compatible with FLI/PAI imaging owing to their appropriate balance between emissive and
603 non-emissive desexcitation pathways, for which only a limited number of synthetic routes was
604 described in the literature.[10,12] This work represents the first proof of concept of a
605 competent PET/PAI/FLI probe with well-balanced imaging properties, which can be coupled
606 to diverse vectors for *in vivo* targeting and thus possesses a strong potential toward clinical
607 translation. Importantly, because this approach was designed to grant the fast and modular
608 functionalization with vectors of the platform at a latest stage, which is crucial for versatile
609 diagnosis and personalized medicine, the present work reaches far beyond cancer diagnosis.
610 Furthermore, probe **27** that bears two anchoring points, also offered the advantage of
611 harnessing bivalency for a more specific targeting. Although **27** initially lacked aqueous
612 solubility, this was successfully overcome by incorporating vectors bearing a hydrophilic
613 spacer like PEG₄. The resulting agent **30** displayed a *clogD*_{7.4} of -3.12, hence making it more
614 likely for translation toward *in vivo* applications. To the best of our knowledge, the sole
615 example of a multimodal PET/PAI/FLI agent described in literature [20], constructed on a
616 croconium vector, capitalizes on its inherent photophysical properties and was radiolabeled
617 through a stable [¹⁸F]F-C bond. Compared to this croconium agent, the probe **27** displayed 1)
618 an appropriate photophysical balance for performing both FLI and PAI, 2) the possibility to
619 access divalence thanks to two vacant positions on the platform, which could be attractive for
620 enhancing its targeting efficiency, 3) the conjugation in the final step which should facilitate
621 the change of vectors to switch to another biological target (versatility in receptor targeting
622 and pathology to be diagnosed).

623

624 **4. Conclusion**

625 In this study, we present a synthetic route for accessing a multimodal imaging probe designed
626 for PET/PAI/FLI applications and evaluation of their optical properties. By exploiting a *N*- to
627 *O*-transposition reaction, we first synthesized a series of meso-*O*-alkyl cyanine-7 derivatives
628 bearing functional groups (azide, alkyne, alkene) of use for further conjugation. These meso-
629 *O*-alkyl cyanine 7 derivatives demonstrated excellent characteristics for fluorescence imaging

630 compared to IR780, with high molar absorptivity and an improved fluorescence quantum
631 yield (>15%). The meso-*O*-alkyl Cy7 derivative bearing an azide was coupled to a highly
632 functionalized *C*-glycosyl platform and successfully ¹⁸F-radiolabelled *via* a [¹⁸F]F-C bond. Its
633 non-radioactive analog, the probe **27** proved to display excellent photophysical properties
634 well-balanced for concomitant fluorescence imaging and photoacoustic imaging. Finally, a
635 late-stage CuAAC coupling of **27** with two model peptides c(RGDfK) was successfully
636 performed, thus demonstrating the feasibility and the versatility of this conjugation step.
637 Altogether, compound **27** undeniably emerged as a promising multimodal PET/PAI/FLI probe
638 foreshadowing of its great potential across a broad spectrum of imaging modalities and
639 applications.

640

641 **CRediT authorship contribution statement**

642 Kamal Jouad: Conceptualization, Methodology, Investigation, Writing - Review & Editing.
643 Emilien Mengel: Investigation, Writing - Review & Editing. Katalin Selmeczi: Methodology,
644 Validation, Writing – original draft, Writing - Review & Editing. Mathilde Bouché:
645 Methodology, Investigation, Writing – original draft, Writing - Review & Editing. Charlotte
646 Collet: Methodology, Writing - Review & Editing. Nadia Pellegrini-Moïse:
647 Conceptualization, Supervision, Visualization, Project administration, Writing – original
648 draft, Writing - Review & Editing. Sandrine Lamandé-Langle: Conceptualization,
649 Supervision, Visualization, Project administration, Writing – original draft, Writing - Review
650 & Editing.

651

652 **Declaration of competing interest**

653 The authors declare that they have no known competing financial interests or personal
654 relationships that could have appeared to influence the work reported in this paper

655

656 **Acknowledgments**

657 The authors gratefully acknowledge the European Regional Development Funds (Programme
658 opérationnel FEDER-FSE Lorraine et Massif des Vosges 2014-2020/“Fire Light” project:
659 “Photo-bio-active molecules and nanoparticles”). We acknowledge The Ministère de
660 l’Enseignement Supérieur et de la Recherche for PhD funding to E. Mengel. We thank S.
661 Parant from PhotoNS platform of the L2CM Laboratory (Université de Lorraine, Nancy,
662 France), T. Gulon from SynBioN - L2CM (Université de Lorraine-CNRS) and F. Dupire from
663 MassLor Platform (Université de Lorraine, Nancy, France) for technical assistance. We thank

664 the NMR Platform of Université de Lorraine (Nancy, France) and NancycloTep, platform
665 member of France Life Imaging network (grant ANR-11-INBS-0006).

666

667 **Appendix A. Supplementary data Supplementary data**

668 Supplementary data to this article can be found online at...

669

670 **References**

671 [1] Klenner M A, Pascali G, Massi M, Fraser B H. Fluorine- 18 Radiolabelling and
672 Photophysical Characteristics of Multimodal PET–Fluorescence Molecular Probes. *Chem.*
673 *Eur. J.* 2021;27:861–876. <https://doi.org/10.1002/chem.202001402>.

674 [2] Vaquero J J, Kinahan P. Positron Emission Tomography: Current Challenges and
675 Opportunities for Technological Advances in Clinical and Preclinical Imaging Systems.
676 *Annu. Rev. Biomed. Eng.* 2015;17:385. [https://doi.org/10.1146/annurev-bioeng-071114-](https://doi.org/10.1146/annurev-bioeng-071114-040723)
677 [040723](https://doi.org/10.1146/annurev-bioeng-071114-040723).

678 [3] Chen G, Li C, Zhang Y, Wang Q. Whole-Body Fluorescence Imaging in the Near-Infrared
679 Window. In: Wei X., Gu B. (eds) *Optical Imaging in Human Disease and Biological*
680 *Research. Advances in Experimental Medicine and Biology*, Springer, Singapore, 2021;3233;
681 p 83. https://doi.org/10.1007/978-981-15-7627-0_5.

682 [4] Lauwerends L J, van Driel P B A, Baatenburg de Jong M J, Hardillo J A U, Koljenovic S,
683 Puppels G, Mezzanotte L, Löwik C W, Rosenthal E L, Vahrmeijer A L, Keereweer S. Real-
684 time fluorescence imaging in intraoperative decision making for cancer surgery. *Lancet*
685 *Oncology* 2021;22:e186. [https://doi.org/10.1016/S1470-2045\(20\)30600-8](https://doi.org/10.1016/S1470-2045(20)30600-8).

686 [5] Zhou J, Jokerst J V. Photoacoustic imaging with fiber optic technology: A review.
687 *Photoacoustics* 2020;20:100211. <https://doi.org/10.1016/j.pacs.2020.100211>.

688 [6] Bossy E, Gigan S. Photoacoustics with coherent light. *Photoacoustics* 2016;4:22.
689 <https://doi.org/10.1016/j.pacs.2016.01.003>.

690 [7] Fu Q, Zhu R, Song J, Yang H, Chen X. Photoacoustic Imaging: Contrast Agents and Their
691 *Biomedical Applications. Adv. Mater.* 2019;31:1805875.
692 <https://doi.org/10.1002/adma.201805875>.

693 [8] Fei G, Maa S, Wang C, Chen T, Li Y, Liu Y, Tang B, James T D, Chen G. Imaging
694 strategies using cyanine probes and materials for biomedical visualization of live animals.
695 *Coor. Chem. Rev.* 2021;447:214134. <https://doi.org/10.1016/j.ccr.2021.214134>.

696 [9] Feng L, Chen W, Ma X, Liu S H, Yin J. Near-infrared heptamethine cyanines (Cy7):
697 from structure, property to application. *Org. Biomol. Chem.* 2020;18:9385-9397.
698 <https://doi.org/10.1039/D0OB01962C>.

699 [10] Exner R M, Cortezon-Tamarit F, Pascu S I. Explorations into the Effect of meso-
700 Substituents in Tricarbocyanine Dyes: A Path to Diverse Biomolecular Probes and Materials.
701 *Angew. Chem. Int. Ed.* 2021;133:6295 – 6306. <https://doi.org/10.1002/anie.202008075>.

702 [11] Ma X, Laramie M, Henary M. Synthesis, optical properties and cytotoxicity of meso-
703 heteroatom substituted IR-786 analogs. *Bioorg Med Chem Lett.* 2018;28:509-514.
704 <https://doi.org/10.1016/j.bmcl.2017.12.001>.

705 [12] Nani R R, Shaum J B, Gorka A P, Schnermann M J. Electrophile-Integrating Smiles
706 Rearrangement Provides Previously Inaccessible C4'-O-Alkyl Heptamethine Cyanine
707 Fluorophores. *Org. Lett.* 2015;17: 302. <https://doi.org/10.1021/ol503398f>.

708 [13] Schnermann M J, Nani R R. PCT Int. WO 2016/072984 A1, 2016.

709 [14] Luciano M P, Crooke S N, Nourian S, Dingle I, Nani R R, Kline G, Patel N L, Robinson
710 C M, Difilippantonio S, Kalen J D, Finn M G, Schnermann M J. A Nonaggregating
711 Heptamethine Cyanine for Building Brighter Labeled Biomolecules. *ACS Chem. Biol.*
712 2019;14:934–940. <https://doi.org/10.1021/acscchembio.9b00122ACS>.

713 [15] Thapaliya E R, Usama S M, Patel N L, Feng Y, Kalen J D, St. Croix B, Schnermann M J.
714 Cyanine Masking: A Strategy to Test Functional Group Effects on Antibody Conjugate
715 Targeting. *Bioconjugate Chem.* 2022;33:718-725.
716 <https://doi.org/10.1021/acs.bioconjchem.2c00083>.

717 [16] Cha J, Nani R R, Luciano M P, Kline G, Broch A, Kim K, Namgoong J M, Kulkarni R
718 A, Meier J L, Kim P, Schnermann M J. A chemically stable fluorescent marker of the ureter.
719 *Bioorg. Med. Chem. Lett.* 2018;28:2741–2745. <https://doi.org/10.1016/j.bmcl.2018.02.040>.

720 [17] Cheng Z, Marriott G. Editorial: Multimodality Molecular Imaging. *Front. Phys.* 2019;7.
721 <https://doi.org/10.3389/fphy.2019.00177>.

722 [18] Ariztia J, Solmont K, Pellegrini Moïse N, Specklin S, Heck M P, Lamandé-Langle S,
723 Kuhnast B. PET/Fluorescence Imaging: An Overview of the Chemical Strategies to Build
724 Dual Imaging Tools. *Bioconjugate Chem.* 2022;33:24.
725 <https://doi.org/10.1021/acs.bioconjchem.1c00503>.

726 [19] Qiu Y, Yuan B, Cao Y, He X, Akakuru O U, Lu L, Chen N, Xu M, Wu A, Li J. Recent
727 progress on near-infrared fluorescence heptamethine cyanine dye-based molecules and
728 nanoparticles for tumor imaging and treatment. *Nanomed Nanobiotechnol.* 2023;e1910.
729 <https://doi.org/10.1002/wnan.1910>.

730 [20] Liu Y, Yang Y, Sun M, Cui M, Fu Y, Lin Y, Li Z, Nie L. Highly specific noninvasive
731 photoacoustic and positron emission tomography of brain plaque with functionalized
732 croconium dye labeled by a radiotracer. *Chem. Sci.* 2017;8:2710.
733 <https://doi.org/10.1039/c6sc04798j>.

734 [21] Ariztia J, Jouad K, Jouan-Hureau V, Pierson J, Collet C, Kuhnast B, Selmezi K, Boura
735 C, Lamandé-Langle S, Pellegrini Moïse N. Clickable C-Glycosyl Scaffold for the
736 Development of a Dual Fluorescent and [18F]fluorinated Cyanine-Containing Probe and
737 Preliminary In Vitro/Vivo Evaluation by Fluorescence Imaging. *Pharmaceuticals*
738 2022;12:1490. <https://doi.org/10.3390/ph15121490>.

739 [22] Vucko T, Ariztia J, Jouad K, Chapeau D, Mourot B, Jouan-Hureau V, Collet C, Boura
740 C, Selmezi K, Pellegrini-Moïse N, Lamandé-Langle S. Cyanine-based [18F]F-C-glycosyl
741 dual imaging probe: Synthesis, physico-chemical characterizations, in vitro binding
742 evaluation and direct [18F]fluorination. *New J. Chem.* 2023.;47:3055 – 3066.
743 <https://doi.org/10.1039/D2NJ06134A>.

744 [23] Richard M, Ariztia J, Lamandé-Langle S, Pellegrini Moïse N. Sugar γ -Amino Acids as
745 Building Blocks for the Synthesis of Cyclic Neoglycopeptides. *Chemistry Select*
746 2018;3:9121–9126. <https://doi.org/10.1002/slct.201802146>.

747 [24] Meldal M, Diness F. Recent Fascinating Aspects of the CuAAC Click Reaction. *Trends*
748 *in chemistry* 2020;2:569-584. <https://doi.org/10.1016/j.trechm.2020.03.007>.

749 [25] Yang J, Karver M R, Li W, Sahu S, Devaraj N K. Metal-Catalyzed One-Pot Synthesis of
750 Tetrazines Directly from Aliphatic Nitriles and Hydrazine. *Angew. Chem. Int. Ed.*
751 2012;51:5222 –5225. <https://doi.org/10.1002/anie.201201117>.

752 [26] Sinha A K, Equbal D, Thiol–Ene Reaction: Synthetic Aspects and Mechanistic Studies
753 of an Anti-Markovnikov-Selective Hydrothiolation of Olefins, *As. J. Org. Chem.* 2019;8:32-
754 47. <https://doi.org/10.1002/ajoc.201800639>.

755 [27] Yang Y, Yu B. Recent Advances in the Chemical Synthesis of C-Glycosides. *Chem.*
756 *Rev.* 2017;117 :12281-12356. <https://doi.org/10.1021/acs.chemrev.7b00234>.

757 [28] Ariztia J, Chateau A, Boura C, Didierjean C, Lamandé-Langle S, Pellegrini Moïse N.
758 Synthesis of Anti-Proliferative [3.3.0]Furofuranone Derivatives by Lactonization and
759 Functionalization of C-Glycosyl Compounds. *Bioorg. Med. Chem.* 2021;45:116313.
760 <https://doi.org/10.1016/j.bmc.2021.116313>.

761 [29] Kapp T G, Rechenmacher F, Neubauer S, Maltsev O V, Cavalcanti-Adam E A, Zarka R,
762 Reuning U, Notni J, Wester H J, Mas-Moruno C, Spatz J, Geiger B, Kessler H. A

763 Comprehensive Evaluation of the Activity and Selectivity Profile of Ligands for RGD-
764 binding Integrins. *Sci. Rep.* 2017;7:39805. <https://doi.org/10.1038/srep39805>.

765 [30] Mahon E, Barboiu M. Synthetic multivalency for biological applications. *Org. Biomol.*
766 *Chem.* 2015;13:10590. <https://doi.org/10.1039/C5OB01357G>.

767 [31] Levitz A, Marmarchi F, Henary M. Synthesis and Optical Properties of Near-Infrared
768 meso-Phenyl-Substituted Symmetric Heptamethine Cyanine Dyes. *Molecules* 2018;23:226.
769 <https://doi.org/10.3390/molecules23020226>.

770 [32] Li D-H, Smith B D, Deuterated Indocyanine Green (ICG) with Extended Aqueous
771 Storage Shelf-Life: Chemical and Clinical Implications. *Chem. Eur. J.* 2021;27:14535.
772 <https://doi.org/10.1002/chem.202102816>

773 [33] Mokrousov M D, Thompson W, Ermilov S A, Abakumova T, Novoselova M V,
774 Inozemtseva O A, Zatsepin T S, Zharov V P, Galanzha E I, Gorin D A, Indocyanine green
775 dye based bimodal contrast agent tested by photoacoustic/fluorescence tomography setup.
776 *Biomed. Opt. Express*, 2021;12:3181–3195. <https://doi.org/10.1364/BOE.419461>.

777 [34] Huang X, Song J, Yung B C, Huang X, Xiong Y, Chen X. Ratiometric optical
778 nanoprobe enable accurate molecular detection and imaging. *Chem. Soc. Rev.*
779 2018;47:2873–2920. <https://doi.org/10.1039/C7CS00612H>.

780 [35] Pu K, Shuhendler A J, Jokerst J V, Mei J, Gambhir S S, Bao Z, Rao J. Semiconducting
781 polymer nanoparticles as photoacoustic molecular imaging probes in living mice. *Nat.*
782 *Nanotechnol.* 2014;9:233–239. <https://doi.org/10.1038/nnano.2013.302>.

783 [36] Bouche M, Puhlinger M, Iturmendi A, Arnirshaghghi A, Tsourkas A, Teasdale I,
784 Cormode D. P. Recent advances in molecular imaging with gold nanoparticles. *ACS Appl*
785 *Mater Inter* 2019;11:28648–28656. <https://doi.org/10.1021/acs.bioconjchem.9b00669>.

786 [37] Lucas T, Sarkar M, Atlas Y, Linger C, Renault G, Gazeau F, Gateau J. Calibrated
787 Photoacoustic Spectrometer Based on a Conventional Imaging System for In Vitro
788 Characterization of Contrast Agents. *Sensors (Basel)* 2022;22:6543.
789 <https://doi.org/10.3390/s22176543>. 10.3390/s22176543.